A comprehensive approach to study stack emissions from a research building in a small urban setting

Abstract

Gaseous emissions from research facilities within an urban environment have not been fully studied. The present study investigates the impacts of stack emissions from a research building in Hong Kong on nearby urban areas. Fifteen chemicals emitted from the laboratories of the building were selected for a year-long air monitoring. Among the 15 chemicals, the levels of NO_2, acetonitrile, and total volatile organic compounds (TVOC) exceeded the predetermined exposure levels. A tracer gas study was performed to identify the dilution factor of the environment and to validate two turbulence models, namely, Renormalized Group (RNG) and Realizable (RLZ) k-ε models. Statistical tests, including geometric mean bias (MG) and factor of two (FAC2), demonstrated that the RNG (MG: 0.88-1.5; FAC2: 0.67-1.14) was better than the RLZ k-ε model (MG: 0.26-0.68; FAC2: 1.47-3.80) for the prediction of pollutant dispersion and concentration distribution but still could not achieve statically sound results. Despite the RNG k-ε model is a popular and economical choice in numerical simulations, careful interpretation of data would be required, and it should also be used

and read in conjunction with air monitoring and tracer gas assessment data as a comprehensive approach when assessing the impact of stack emissions in an urban setting.

1. Introduction

Similar to other megacities in developed countries, Hong Kong is a densely populated city with over 7.4 million people inhabiting 1,106.34 km² of land (Census and Statistics Department of Hong Kong, 2018). A mix of different types of buildings, built for different purposes, within a small urban environment is common and somehow inevitable. Given the high density of buildings and closeness of road networks, the land-use types, vehicle emissions, and exhaust stacks of industries and research facilities are likely to adversely affect the health of local inhabitants.

Microclimate elements such as wind-speed, wind direction, air-flow pattern, and air temperature are also influenced by the closeness of the buildings and width of the roads in the vicinity (Ai & Mak, 2016). Low wind speeds can hinder the dispersion of air contaminants in an urban environment, and this effect is further exacerbated by closely-spaced buildings (Du & Mak, 2018; Du, Mak, & Li, 2019; Ignatius, Wong, & Jusuf, 2015). The distribution and dilution of air pollutants in an urban locality are affected by the air-flow (Dai, Mak, Ai, & Hang, 2018), whose pattern around the buildings significantly affects the overall air quality of the area (Borrego et al., 2006; Yuan, Ng, & Norford, 2014). To dilute the air pollutants in an urban locality, wind penetration should be increased through a careful town planning, considering the geometry of the urban setting (Ai, Mak, & Lee, 2016; Fang et al., 2019).

Unlike industrial or traffic emission, gaseous emission from research facilities are difficult to characterize owing to the diverse processes, the changing nature of research, and the use of different chemicals at different times (Ballinger & Larson, 2014). The emission pattern is irregular and heavily relies on the research or laboratory activities at a given time. Moreover, the emission of toxic chemicals from these facilities can adversely affect the health of people in the surrounding areas. Lateb, Masson, Stathopoulos, and Bédard (2011) evaluated the effects of stack height and exhaust velocity on the dispersion of air pollutants in the wake of a building by using a computational fluid dynamics (CFD) model validated by a wind tunnel study. Yassin (2013) investigated the wind flow and pollutant dispersion from rooftop stacks near the wake of a building by conducting a wind tunnel experiment. However, stack emissions of research facilities or laboratory buildings and their impact on air quality within a real, small, and complex urban setting have not been separately investigated and fully studied.

To assess the impacts of gas emissions, full-scale field measurement of air quality is a straightforward method that identifies the concentration and dispersion patterns of air pollutants in a defined environment. However, this method is expensive, and it is not always feasible to perform continuous air sampling for a long period of time. The accuracy of the results is also subject to the placement and number of sampling

locations. Sampling also involves high installation- and laboratory-analysis-costs. It is almost impossible to reproduce experimental data in full-scale air monitoring because of the uncontrollable wind and weather conditions, changing wind directions, variable pollutant emissions from difference sources and their dispersion patterns (Cremades, 2000; Dai et al., 2018). Therefore, the numerical methods and CFD techniques have been increasingly used for this purpose.

CFD can generate reproducible results of air-flow and dispersion patterns around buildings, which are crucial to assess the air quality, comfort, and health of the residents and the people working in the vicinity of the pollution source (Lateb, Masson, Stathopoulos, & Bedard, 2013). Moreover, CFD is less expensive than actual field measurements and wind-tunnel experiments, and it would not be affected by uncontrollable and diverse nature and meteorological conditions (Blocken, Stathopoulos, Saathoff, & Wang, 2008). However, the accuracy of CFD simulation results can be affected by grid resolution, boundary conditions, geometrical representation, computational parameters and, most importantly, by the selection of turbulence models (Lateb et al., 2013; Tominaga & Stathopoulos, 2013).

The Reynolds-averaged Navier-Stoke (RANS) is a commonly used approach to solve turbulence problems and it focuses on the mean flow properties of turbulence (Blocken, 2015; Xia, Niu, & Liu, 2014). It is also used to examine the wind flow

around buildings (Du et al., 2019). However, RANS tends to over-predict the turbulent

kinetic energy on the windward side of the building, and overestimate the reattachment

lengths on the roof and the wake region of the building (Lübcke, Schmidt, Rung, &

Thiele, 2001; Mochida & Lun, 2008). Notwithstanding the tendency to overestimate

turbulence formation on the frontal area of the building (Burman & Jonsson, 2015),

RANS can be modified to calculate microscale wind flow in an urban setting (X.-X. Li,

Liu, Leung, & Lam, 2006). Therefore, it remains popular because of its low cost in

terms of computational resources, computing time, and hardware cost.

Among different RANS approaches, the k-ε turbulence models are frequently used.

They include the Standard k-ε model (SKE), the Renormalization Group (RNG) k-ε

model, and the Realizable (RLZ) k-ε model. According to Tominaga and Stathopoulos

(2013), the over-prediction of turbulence kinetic energy in the frontal areas of

buildings contributes to the poor performance of SKE models in the description of

separation flow. In addition, the performance of SKE depends on the turbulent Schmidt

number to solve the dispersion equation (Gousseau, Blocken, Stathopoulos, & van

Heijst, 2011). Compared to the transient models such as the Direct Numerical

Simulation (DNS) and the Large Eddy Simulation (LES), the prediction of air pollutant

concentration by SKE is the least coincidental with experimental data (Gousseau et al.,

2011). Therefore, since SKE would provide a poor performance for complex flow, this

method was not selected for the present study.

The RLZ k-ε model can provide a more accurate concentration distribution trend of the lower region between two buildings. However, it tends to underestimate the lateral dispersion of pollutants and overestimate the reattachment lengths of the roof and wake region of buildings (Lateb et al., 2013). Nevertheless, the RNG k-ε model provides a more accurate description of complex processes compared to other k-ε models (Canepa, 2004) because it introduces additional strain-dependent terms into the calculation of turbulent dissipation rate (ε) (Du et al., 2019). Therefore, it provides more accurate and reliable results for a wider class of flows (Lateb et al., 2013), and more realistic outcomes for rapidly strained and swirling flows (Ai & Mak, 2013), turbulence flow, and concentration diffusion in the building-wake (Liu & Niu, 2016). Compared with the SKE and RLZ k-ε model, the RNG k-ε model provides higher consistency with the experimental results from wind-tunnel studies (Lateb et al., 2013; Tominaga & Stathopoulos, 2009), and it considers turbulence flow and flow recirculation within street canyons and urban areas (Chan, Dong, Leung, Cheung, & Hung, 2002; Koutsourakis, Bartzis, & Markatos, 2012).

Only a limited number of CFD studies on complex urban settings have been validated by field measurements (Dadioti & Rees, 2017). In addition, the impacts of emissions from research facilities within a small urban setting have not been

thoroughly investigated. Therefore, the present study analyzed the emissions from a research building of a local university in Hong Kong and evaluated the related impacts on the nearby area. The effects of approaching wind velocities on pollutant dispersion within a small urban setting and building arrays were also identified. The small urban setting of this study includes an area of a few hundred meters around the studied building, where the interaction of plume and flow field would be perturbed by the building obstacles according to Tominaga and Stathopoulos (2013).

To achieve the aim of this study, the air emissions from the building were monitored for selected chemicals during one year, and a tracer gas study was conducted. The tracer gas analysis was used to identify dilution factors in the environment and subsequently to validate the CFD models. The data from air sampling and tracer gas analysis were compared with the simulation results from the RNG and RLZ k-ε models in terms of pollution dispersion patterns and changes in the wind-speeds within building arrays of the selected environment.

2. **Methodology**

2.1 Site Description

The ZS Building is a research center of a university in the urban area (near Homantin) of the Kowloon peninsula in Hong Kong (Fig. 1). There are 19 emission stacks installed on the roof of the building. Each of these stacks is connected to a

laboratory with a chemical fume cupboard, which discharges chemical fumes or vapors into the atmosphere. The Inno Tower (IT) is a 15-story academic building in the same university, and it is located about 100 m southeast of the ZS Building (Fig. 1). Though IT does not house any chemical laboratory, the building is ventilated by mechanical ventilation and air-conditioning (MVAC) system, and the fresh air intake of IT is located on its roof, facing the ZS Building.

Figure 1. Study location in the Kowloon Peninsula of Hong Kong

The private Residence W is located approximately 100 m northwest of the ZS Building. It comprises five 12-story residential buildings arranged in a 'U' shape around a central space with a podium on which recreational amenities, including a swimming pool and playgrounds, are located. Every building in the complex is separated from the adjacent building by a gap of approximately 5 m, except Blocks A and B, which are joint without any gap between them. Gao, Niu, Perino, and Heiselberg (2008) observed that source location and wind direction can affect the dispersion pattern of air pollutants. As Blocks B, D, and E are located closer to the ZS

Building, they are more likely to be affected by the studied gaseous emission. Fig. 2 shows a wind rose diagram, which illustrates that the prevailing winds in the study area blow from southeast at about 40% of the time (Hong Kong Observatory, 2017). Therefore, Residence W, which is northeast of the ZS Building, is situated in the wake region of the building and is more susceptible to the impact of stack emission for at least 40% of time throughout the year.
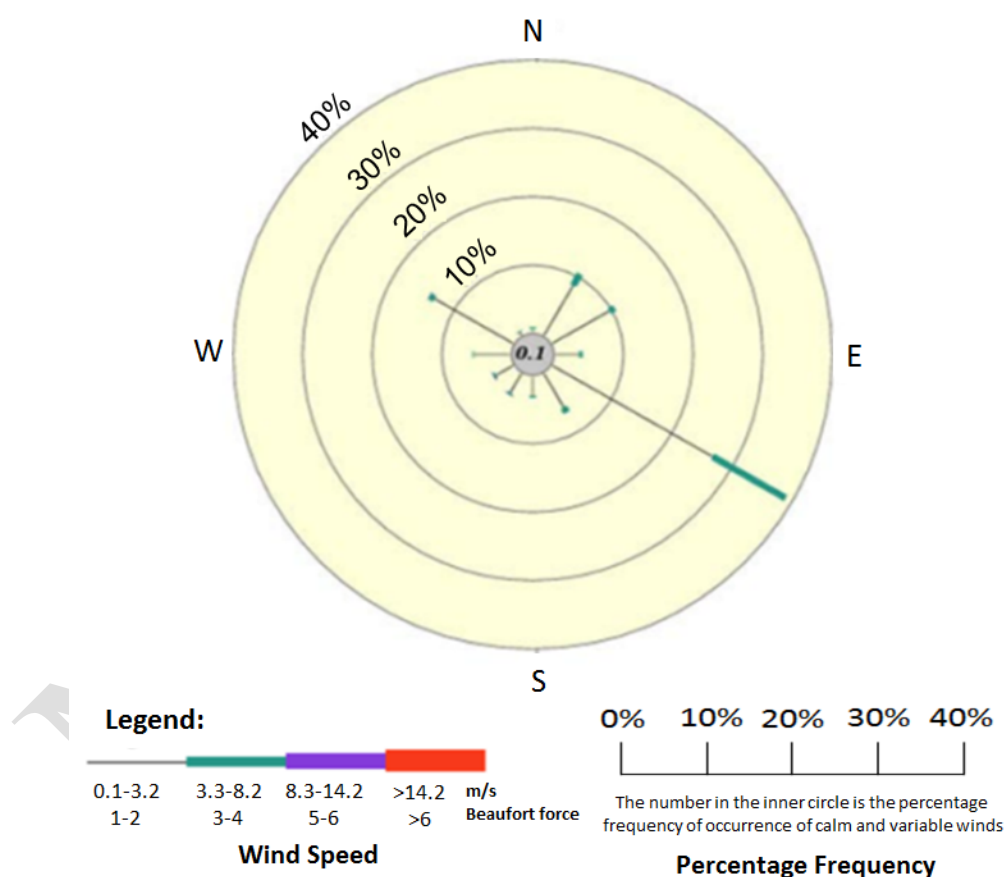
Figure 2. Wind rose diagram of 2016 for areas near the ZS Building (Hong Kong Observatory, 2017)

To identify the possible chemical emissions from the laboratories, the author interviewed laboratory operators. Fifteen chemicals that can lead to toxic fumes or vapors during reactions or upon exposure to air under normal room temperature and

conditions were selected for the year-long air quality monitoring.

In Hong Kong, the Air Pollution Control Ordinance (APCO) enforced by the Hong Kong Environmental Protection Department (HKEPD) is the only regulator of outdoor air pollution. The HKEPD regulation defines the statutory Air Quality Objectives and stipulates the maximum allowable concentrations for typical air pollutants, of which nitrogen dioxide (NO_2) and carbon monoxide (CO) are relevant to this study. The exposure limit of formaldehyde is based on the Indoor Air Quality (IAQ) objectives set by the Indoor Air Quality Management Group (IAQMG) of HKEPD in 2003 (Indoor Air Quality Management Group, 2003). For air pollutants not mentioned by the APCO and the IAQ objectives, recognized international standards were used. The exposure (acute and chronic) parameters of chemicals are varied, and they were determined and analyzed based on the guidelines of international authorities. Table 1 lists the monitored chemicals and their corresponding exposure standards.

Pollutant	Parameter(s)	Exposure Limits		Reference
		(µg/m³)	(ppb)	
Acetone	Acute	66,500	26,000	(ATSDR, 1994)
	Chronic	33,200	13,000	(ATSDR, 1994)
Acetonitrile	1-hour	21,294	13,000	(USEPA, 2014)
	Chronic	60	36	(USEPA - Integrated Risk Information System (IRIS), 1999)
Carbon monoxide	1-hour	30,000	26,200	(HKEPD, 2015)
	8-hour	10,000	8,700	(HKEPD, 2015)
Chloroform	Acute	490	100	(ATSDR, 1997)
	Chronic	98	20	(ATSDR, 1997)
Dichloromethane	24-hour	3,000	860	(World Health Organisation, 2000)
	Chronic	600	170	(USEPA - Integrated Risk Information System (IRIS), 2011)
Formaldehyde	Acute	100	81	(Indoor Air Quality Management Group, 2003)
	Chronic	100	81	(World Health Organisation, 2000)
Hydrochloric acid	Acute	2,100	1,410	(OEHHA, 2016)
	Chronic	20	13	(USEPA-Integrated Risk Information System (IRIS), 1995)
Methanol	Acute	28,000	21,370	(OEHHA, 2016)
	Chronic	20,000	15,260	(USEPA- Integrated Risk Information System (IRIS), 2013)
n-hexane	Acute	Not available	Not available	Not available
	Chronic	700	20	(USEPA-Integrated Risk Information System

				(IRIS), 2005)
Nitric acid	Acute	86	33	(OEHHA, 2016)
	Chronic	Not available	Not available	Not available
Nitrogen dioxide	Acute	200	110	(HKEPD, 2015)
	Chronic	40	21	(HKEPD, 2015)
Tetrahydrofuran	Acute	Not available	Not available	Not available
	Chronic	2,000	680	(USEPA-Integrated Risk Information System (IRIS), 2012)
Toluene	Acute	7,540	2,000	(ATSDR, 2017)
	Chronic	5,000	1,330	(USEPA - Integrated Risk Information System (IRIS), 2005)
Trichloroethane	Acute	10,910	2,000	(ATSDR, 2006)
	Chronic	3,820	700	(ATSDR, 2006)
TVOC	Acute/Chronic	1,000	435	(Nathanson, 1995)
	8-hour (mean)	600	261	(Indoor Air Quality Management Group, 2003)

*Table 1.   List of monitored chemicals and their exposure limits*

2.2   Air Sampling

To identify the impacts from the emissions, air samples were obtained from

Residence W and from the fresh air intake of IT. The sampling points were distributed

in different locations and levels of Blocks B, D, and E at Residence W, and in the roof of

IT. The samples for air quality monitoring at Residence W were obtained at different

heights, namely at the roof-, mid- (10th floor), and podium-levels. However, due to the

inaccessibility, sampling at the mid-level of Blocks B, D, and E could only be conducted

at the back stairwells located in the wake of Residence W. There is an increased risk of contamination near the leeward façade due to the fluctuating air stream and reverse flow, which lead to the accumulation of gaseous pollutants in these areas (Mu, Gao, & Zhu, 2016). The sampling points allotted in the wake of Residence W should help reflect and verify this phenomenon. Fig. 3 illustrates the distribution of the sampling points in Residence W and IT.
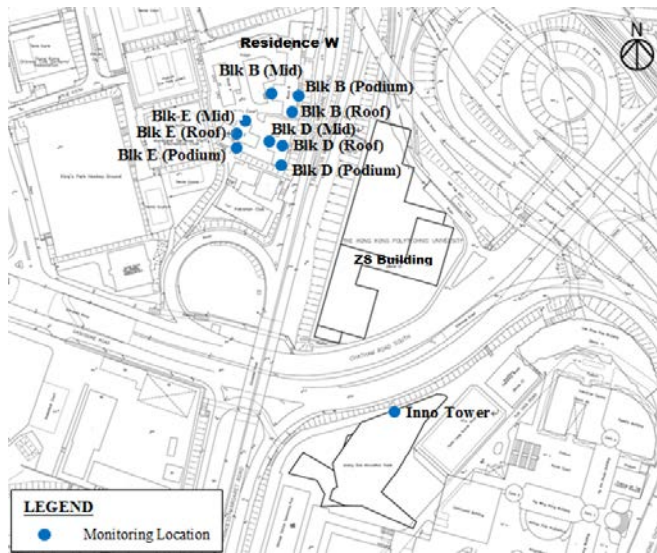
(a)
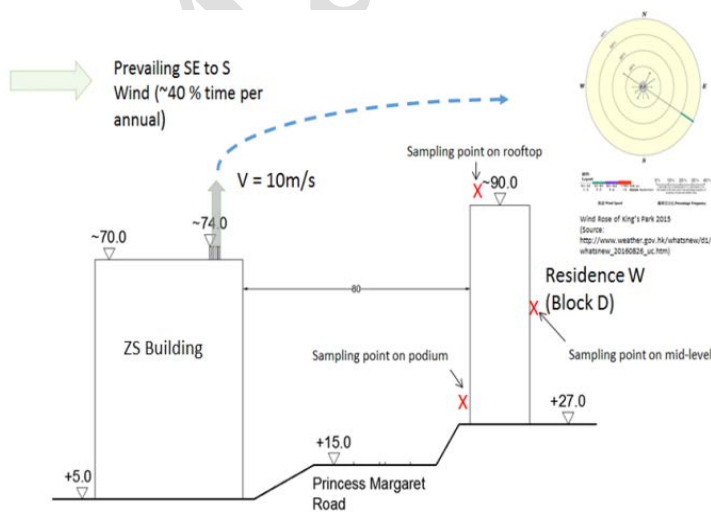
(b)

Figure 3. Air monitoring locations: (a) top-view of sampling locations in Residence W and IT; (b) side-view of ZS Building and sampling points in Residence W.

The effects of seasonal changes in wind direction and meteorological conditions were determined based on the changes in ambient concentration of the selected chemicals. This analysis considered the operation of the chemical fume cupboards in the laboratories of the ZS Building under different weather conditions and in different seasons of the year. The analysis was named baseline air quality monitoring when the fume cupboards were not in operation, and operational air quality monitoring when they were in operation. The results were then checked against the exposure criteria shown in Table 1 to determine the extent of the problem. Air samples were collected in accordance with the reference methods and the nature of the chemicals as listed in Table 2. During the sampling, ambient weather conditions such as air temperature, wind speed, wind direction, and relative humidity were also measured and recorded.

Chemicals	Reference Method	Sampling Time	Reporting Limit
Acetone	USEPA Method TO-15	1 hour	100 ppb (20 ppb*)
Acetonitrile	USEPA Method TO-15	1 hour	100 ppb (20 ppb*)
CO	NDIR Analyzer	1 hour	0.4 ppm
Chloroform	USEPA Method TO-15	1 hour	1 ppb
Dichloromethane	USEPA Method TO-15	1 hour	1 ppb
Formaldehyde	USEPA Method TO-11A	1 hour	20 ppb
Hydrochloric acid	NIOSH Method 7903	2 hours	0.05 mg/m^3 at 0.5 L/min for 120 mins (0.037 mg/m^3*)
Methanol	USEPA Method TO-15	1 hour	100 ppb (20 ppb*)

Chemicals	Reference Method	Sampling Time	Reporting Limit
n-hexane	USEPA Method TO-15	1 hour	1 ppb
Nitric acid	NIOSH Method 7903	2 hours	0.05 mg/m^3 at 0.5 L/min for 120 mins (0.037 mg/m^{3}*)
NO$_2$	Chemiluminescence Analyzer	1 hour	10 ppb
Tetrahydrofuran	USEPA Method TO-15	1 hour	100 ppb (20 ppb*)
Toluene	USEPA Method TO-15	1 hour	1 ppb
Trichloroethane	USEPA Method TO-15	1 hour	1 ppb
TVOC	Photo-Ionization Detection	1 hour	1 ppb

Note:

*   Value in ( ) refers to the lowest unaccredited reporting limit of the laboratory testing instrument. Concentrations reported below the accredited reporting limit are for reference only.

Table 2.   ***Analytical methods and reporting limits for the monitoring of selected chemicals***

There were 12 baseline and 37 operational air quality monitoring events conducted throughout the year. The monitoring events were not conducted on the same day so the likely residual effect of the operational air monitoring would be excluded from the baseline air monitoring. In addition, before the baseline monitoring, stacks were purged with air. Thereafter, the main power supply of all chemical fume cupboards in the ZS Building was shut down for at least two hours before the sampling of the baseline air monitoring. In the operational air quality monitoring, all laboratories in the ZS Building were visited, and all chemicals used in these laboratories were identified. The purpose of these visits was to link the pollutants with the chemicals used in the laboratories, and to identify the key pollutants and the respective levels of chemicals

emitted inside the fume cupboards.

The presence of typical urban air pollutants, such as NO_2, CO, and TVOC, in the samples of the sensitive recipient areas could not be assumed to be solely derived from the stack emissions. In this study, a tracer gas was used to identify the pollution source and the dilution factors in the environment. Sulphur hexafluoride (SF_6), which is a synthetic gas that normally does not exist in the atmosphere, was used as the tracer. To achieve a 10,000 ppm (i.e., 1.0 %v/v) concentration of SF_6 at the stack discharge, the discharge rate of SF_6 gas in the fume cupboard was maintained at 78 L/min or higher. The discharge duration was 30 minutes. SF_6 was released at a constant flow rate from the fume cupboard. Table 3 and Fig. 4 show details of the sampling locations for the tracer gas study.

Monitoring Locations		Sampling Points
A	Inside the fume cupboard of a laboratory in the ZS Building	At the exhaust duct inlet of the fume cupboard
B	Inside the stack linked to the fume cupboard, on the roof-top of the ZS Building	At the stack after the extraction fan
C	ZS Building	Roof (downstream)
D1		Podium level (windward)
D2	Block D of Residence W	Mid-level (leeward)
D3		Roof (windward)

Table 3.   Tracer gas monitoring and sampling locations
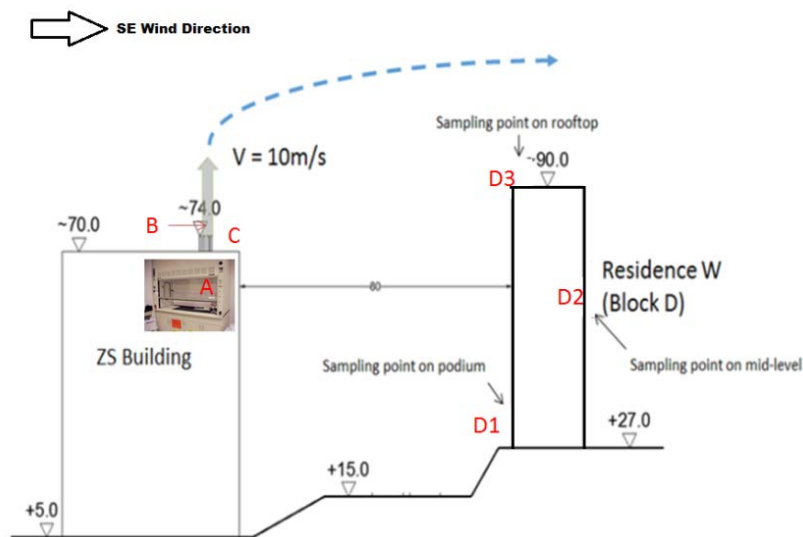
Figure 4. Tracer gas monitoring and sampling locations

As SF_6 is a potent greenhouse gas with a high global warming potential (Dervos & Vassiliou, 2000), its use and release in the environment for a full-scale tracer gas study should be carefully planned and performed in an environmentally-friendly and responsible manner. Due to the constraints on workforce and sampling equipment, only a limited number of sampling stations were established in this study.

Eight consecutive 5-minute air samples were collected at the roof of the ZS Building (Point C); and at the podium (Point D1), mid-level (Point D2), and roof (point D3) of Block D when the southeast wind was dominant and Residence W was downstream of the ZS Building. The ambient temperature and the in-stack flue gas temperature were recorded once in every 5 minutes throughout the whole experimental period. The temperature difference between the averaged ambient and in-stack flue gas temperatures would be used to determine if consideration of the thermal and buoyancy effect in CFD simulations is needed. To obtain more reliable results in a stabilized environment, the first two 5-minute air samples were discarded, and the results from the other six 5-minute air samplings were used to provide the average SF_6 concentration over 30 minutes. From the ZS Building, one sample was collected at the exhaust air duct of the fume cupboard (Point A) for 30 minutes, and the other air sample was collected inside the emission stack on the roof (Point B) for 40 minutes to allow the tracer gas to fill up the space inside the exhaust duct and the stack. The dilution factor can be calculated at a particular location as $D = Ce/C$, where Ce is the tracer gas concentration at the exhaust outlet, and C is its concentration at the receptor.

2.3 CFD Modelling

The study location is an urban area where the wind flow is greatly affected by the surrounding buildings. Therefore, to capture representative wind conditions of the

surrounding area, all buildings in a distance of 8H from the study area, where H is the

height of the tallest building (85 m) in the study area, were included in the domain.

Furthermore, to ensure that the study area is not affected by the domain boundaries, the

domain size was determined in accordance with the COST Action 732 (Franke,

Hellsten, Schlünzen, & B. Carissimo, 2007), and the area of interest was extended from

the boundary of the study area in the four cardinal directions to a distance of at least

15H. The domain height was set to 700 m (8H), which is high enough to cover the inlet

wind profile of the study area from the Planning Department of Hong Kong (Fig. 5),

and it provides enough space for the flow development. The wind profile (Fig. 5) in

Hunghom, southeast of the study area, was selected as the inlet of the model. For areas

outside the building group of the study, only the terrain profile was adopted, to

minimize the blockage effect (Ai & Mak, 2014). Fig. 6 illustrates the study domain in

the ANSYS Fluent 18.2 environment, with a picture of the urban area. According to

Blocken, Stathopoulos, and Carmeliet (2007), horizontal homogeneity can be achieved

when the profiles of inlet, approaching, and incident flow are the same. In this context,

the wind speed and turbulence intensity profiles provided by the Planning Department

of Hong Kong, and the turbulence parameters of adjacent areas, including Tsim Sha

Tsui and Hunghom, were nearly the same. Therefore, the horizontal homogeneity of

the flow field is considered satisfactory, and there is no indication of artificial

acceleration is in the flow field.
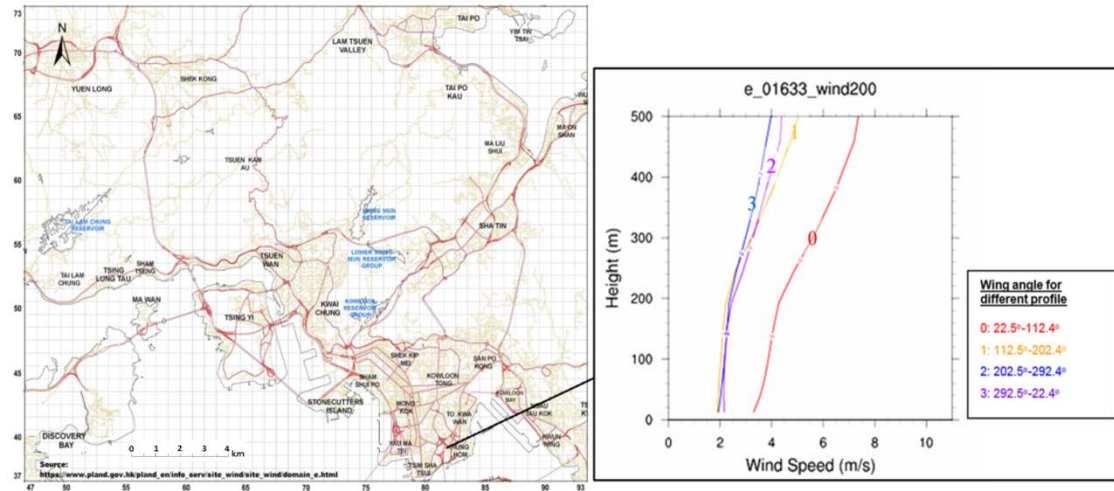
Figure 5. ***Wind profile of the study area, Hunghom, by the Planning Department of Hong Kong***

Figure 6. ***Domain of the study area***

The ANSYS Fluent 18.2 was used to generate the mesh for the modelling and simulations. The mesh sizes ranged from 0.02 m to 1.66 m. Finer meshes of 0.02 m were used for buildings and areas adjacent to the emission stacks to accurately capture the change of turbulence intensity, and the turbulence viscosity in these areas. The fine meshes also help predict the flow and pressure distribution, as demonstrated by Mirzaei and Rad (2013). In contrast, coarser meshes ranging from 0.9 m to 32.9 m were generated for terrains with a maximum growth ratio of 1.2 in adjacent cells. In the

RANS simulations, prediction results do not change significantly with finer grids, according to Tominaga & Stathopoulos (2012). Therefore, a standard grid with 17,367,799 tetrahedral cells was adopted instead of a finer grid, which would have required a significantly longer computing time. Moreover, a prism layer of 2 m above the ground in the entire CFD domain (four layers, each of 0.5 m thickness) was incorporated in the mesh to better capture the approaching wind at the pedestrian level. According to Celik, Ghia, Roache, and Christopher (2008), for each equation solved, an iterative convergence with a reduction of at least three orders of magnitude in the normalized residuals should be ensured before the discretization error is estimated. In the present study, converged solutions were assumed when the scaled residuals reached 10^{-3} for continuity and 10^{-4} for mass conservation, $u, v, w, k,$ and ε. For the RNG k-ε model in the present study, it took more than 12,000 iterations for all variables to become constant or oscillate around a constant value. Despite the residuals for several variables could not reach 10^{-5} or lower, the simulated concentration of SF_6 was virtually constant with a very small oscillation around 3.0×10^{-5} while the residuals continuity and k became stabilized at around 1.25×10^{-4} and 4.8×10^{-5}, respectively, for more than 2,000 iterations. As for the RLZ k-ε model, all residuals, including the concentration of SF_6, became stabilized around the 9,000th iterations, and they remained constant for over 6,000 iterations. As convergence down to very small criteria would result in largely

increased computing time, practicable convergence criteria were selected to obtain quality results in the least possible computing time.

The estimated pollutant concentration by both RANS simulation approaches were compared to the results from the tracer gas study, which was performed when the southeast wind was dominant and Residence W was downstream and in the wake of the ZS Building. To simulate the conditions of dominant southeast wind, the wind angle 1 (Fig. 5) was imposed. No-slip conditions and standard wall functions were assumed for the building surfaces and the terrain in the computational domain. References were made to the updated Davenport roughness classification suggested by Wieringa (1992) and the study conducted by Blocken, Janssen, and van Hooff (2012) in determining the appropriate roughness length (z_0) for the surroundings of the study area. Parameters such as roughness height (k_s) and roughness constant (C_s) were determined to satisfy the relationship: $k_S = 9.793\ z_0/C_s$ derived by Blocken et al. (2007). In the present study, the z_0 of the terrain was 0.03 according to the Davenport roughness classification proposed by Wieringa (1992). As for the building surfaces, uniform sand-grain roughness of façades and roofs was employed. The C_s of 0.5 and k_s of 0.1 were used, and z_0 of 0.005 was derived from the above equation. To maintain the accuracy of CFD simulations, Blocken et al. (2007) also suggested the distance from point P to the wall (y_P) should be larger than k_S since it is not physically meaningful to have a mesh size with wall-adjacent

cell smaller than the roughness height.

The wind direction was southeast, and the wind-speeds were as shown in Fig. 5. Therefore, the inflows were over the eastern and southern boundaries, and the western and northern boundaries were modelled as pressure outlets. The sky of the domain was modelled as a mirror plane or a symmetrical surface, while the emission stack (C9) was modelled with a velocity inlet of 2.7 m/s, according to the onsite measurement. The mixture of SF_6 and air with species mass fraction of $SF_6 = 0.002823$ was input as the material emitted from C9. In accordance with Section 6.3.2.1 of the ANSYS Fluent Release 14.5 User's Guide, "Intensity and Viscosity Ratio" should be chosen for k-ε models (ANSYS FLUENT 14.5, 2012). The turbulence intensity ratio and the turbulence viscosity ratio were determined by the Reynolds number and the Site Wind Availability Data from the Planning Department of Hong Kong. The turbulence intensity ratio can also be determined by the equation: $I = 0.16 \, (ReD_H)^{-1/8}$(ANSYS FLUENT 14.5, 2012). Moreover, the turbulence viscosity ratio, μ_t/μ, is directly proportional to the turbulent Reynolds number, i.e., $Re_t = k^2/\varepsilon v$, at free stream boundaries. At the free-stream boundaries of most external flows, μ_t/μ is fairly small. Typically, the turbulence parameters are set below 10.

According to Liu et al. (2018), SKE fails to predict the reverse flow on the roof of buildings due to the over-prediction of turbulence kinetic energy at the impingement

region of the windward wall. Moreover, SKE is also insufficient to calculate the local pressure distribution in an urban environment (Shirzadi, Naghashzadegan, & A. Mirzaei, 2018). In this context, RNG and RLZ k-ε models were adopted to investigate the results of windward concentration of the tracer gas. The simulated concentration of SF_6 on building roof, and the wake recirculation and vortex shredding behind Residence W were generated by different turbulence models and compared with the tracer gas results to identify the optimum models for this urban setting. Simulations were conducted with the commercial CFD program ANSYS Fluent 18.2. A turbulent Schmidt number (S_{Ct}) of 0.7 was used since it has been adopted in most CFD studies for turbulent mass diffusion (Tominaga & Stathopoulos, 2007). The results from simulating the position of the far downwind of a rectangular building agrees well with experimental data by using k–ε models, with S_{Ct} equal to 0.7 (Y. Li & Stathopoulos, 1997).

SIMPLE pressure-velocity coupling and second-order discretization schemes were used to enhance precision. Thermal and buoyance effects were not actively considered in the study for a number of reasons. First, according to Niu and Tung (2008), the turbulence of a high wind-speed in the study area which exceeds 0.9 m/s, such as in this case, overwhelms the influence of a thermal force. Second, the stack was connected to a chemical fume cupboard that directly exhausts fumes and vapors, where no heating

process was involved. Third, the temperature inside the emission stack and the ambient

temperature outside the stack were measured and found to be roughly the same (the

temperature difference was 0.1°C or 0.1K). A non-dimensional parameter, Richardson

number (Ri), could be used to represent the effect of buoyancy on flow shear

(Bradshaw, 1969). Ri can be defined as $Ri = Gr/Re^2$, where Gr is the Grashof number,

and Re is the Reynolds number. In the current study, the Re is 5.99×10^5, while the Gr

for a case with a small temperature difference of less than 3K (or 3°C) is 3.05×10^{10}

(Garbrecht, 2017). The calculated Ri would be 0.085 that is smaller than 0.1. Since

natural convection (buoyancy) is negligible when Ri <1, it was not necessary to

consider the thermal and buoyance effects in the simulation.

Validation of numerical results from the tracer gas study is essential to create

confidence in the prediction. Therefore, the geometric mean bias (MG) and the fraction

of predictions within a factor of two of observations (FAC2) were used in this study, as

suggested by Chang and Hanna (2004). These two statistical tools were selected because

FAC2 is more robust, since it is insensitive to the distribution of variables under

evaluation, and MG is also considered appropriate for dispersion models where the

concentrations often vary by multiple orders of magnitude (Chang & Hanna, 2004). The

acceptable ranges of MG (0.7-1.3) and FAC2 (0.5-2) suggested by Tewari et al. (2010)

were adopted.

3. **Results**

 The comparison between the air quality monitoring outcomes and the predetermined exposure limits listed in Table 1 revealed that the measured concentrations of all selected chemicals were generally within the permissible exposure limits, with the following exceptions:

i. The level of NO_2 measured at all sampling locations, for both baseline and operational air monitoring events, exceeded the chronic exposure criteria.

ii. Occasional excursions above the acute exposure criteria for TVOC were identified in the mid-level of Block D and all levels of Blocks B and E in Residence W.

iii. Occasional excursions above the chronic exposure criteria for acetonitrile were observed in all sampling locations in Residence W, and during three episodes in IT.

 Since the predetermined exposure levels for the remaining chemicals were not exceeded, the following discussions focus only on NO_2, TVOC, and acetonitrile.

3.1 Nitrogen dioxide (NO_2)

 The operational air monitoring results revealed that the mean NO_2 levels in all sampling locations ranged between 23.8 ppb and 25.2 ppb, and they exceeded the chronic criterion (21 ppb) set by the HKEPD (2015). The NO_2 levels measured in the

baseline air monitoring ranged between 23.8 ppb and 24.9 ppb, which also exceeded the chronic criterion. According to the site measurement data and the wind direction obtained from the Hong Kong Observatory, it was observed that the mean NO_2 levels exceeded the chronic criterion irrespective of the wind direction in the adjacent areas during the monitoring.

Comparing the monitoring results with the annual NO_2 level of 29 ppb recorded in 2016 by the nearest Air Quality Monitoring Station (AQMS) (HKEPD, n.d.), the average NO_2 levels measured in both baseline and operational monitoring were similar to that of the reported ambient background levels. Therefore, it was concluded that the exceeding NO_2 pollution in Residence W and IT were possibly caused by background contributions of the affected area and not by a single emission source from the ZS Building.

3.2 TVOC

Fig. 7 shows the TVOC concentration in the baseline (Fig. 7a) and operational air monitoring for IT (Fig. 7b), and Blocks B (Fig. 7c), D (Fig. 7d), and E (Fig. 7e) of Residence W. Fig. 7f combines all the results of TVOC levels obtained from the baseline and operational air monitoring, which show a similar trend. They both had TVOC peaks slightly higher than 400 ppb in the late summer and early autumn. These results indicate that the environmental TVOC concentration was nearly steady and

uniform over the area most of the time. The pre-existing TVOC could be one of the main contributing factors to the TVOC readings in both baseline and operational air monitoring. However, referring to Fig. 7f, a gap between the operational and the baseline air monitoring was identified in June and July. As laboratory activities were still in progress during the period of operational air monitoring, a correlation between the activities in the ZS Building and higher TVOC readings in Residence W and IT during that period is possible.
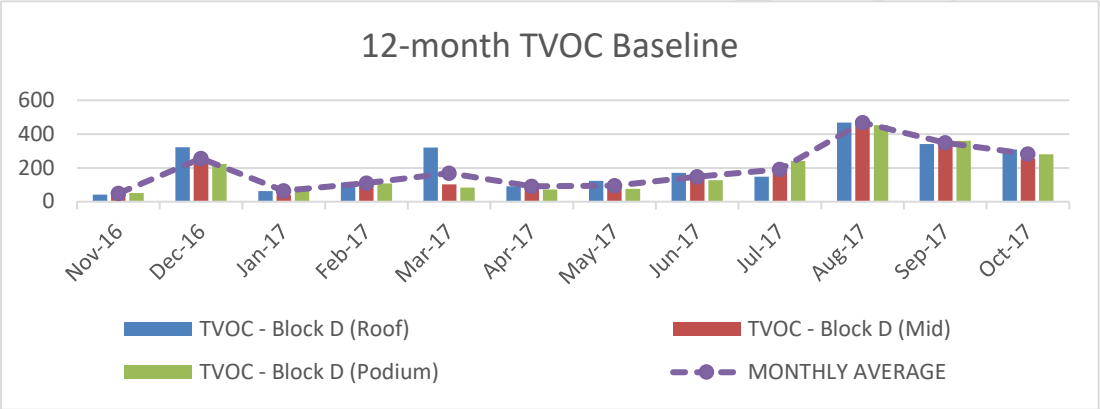
Figure 7a.   Twelve-month total volatile organic compounds (TVOC) baseline level
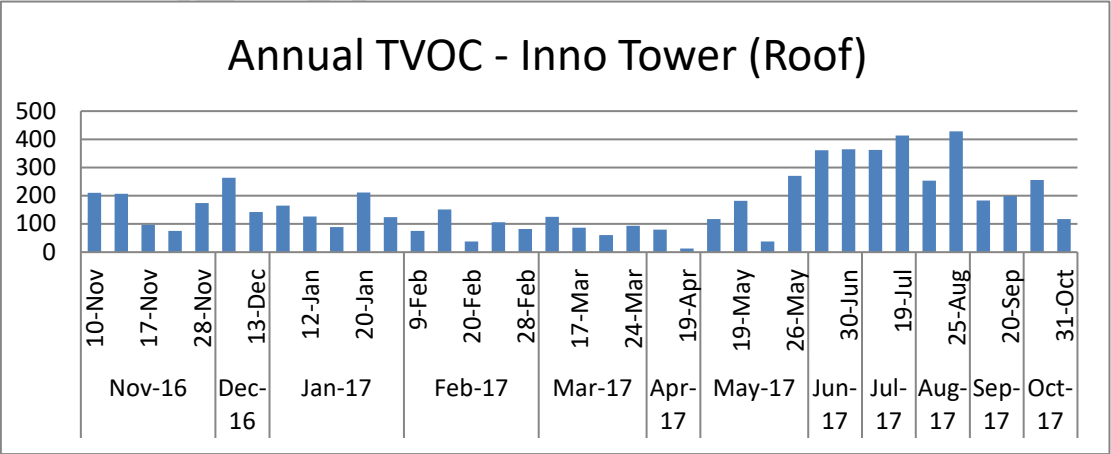
Figure 7b.   Monthly levels of TVOC in IT
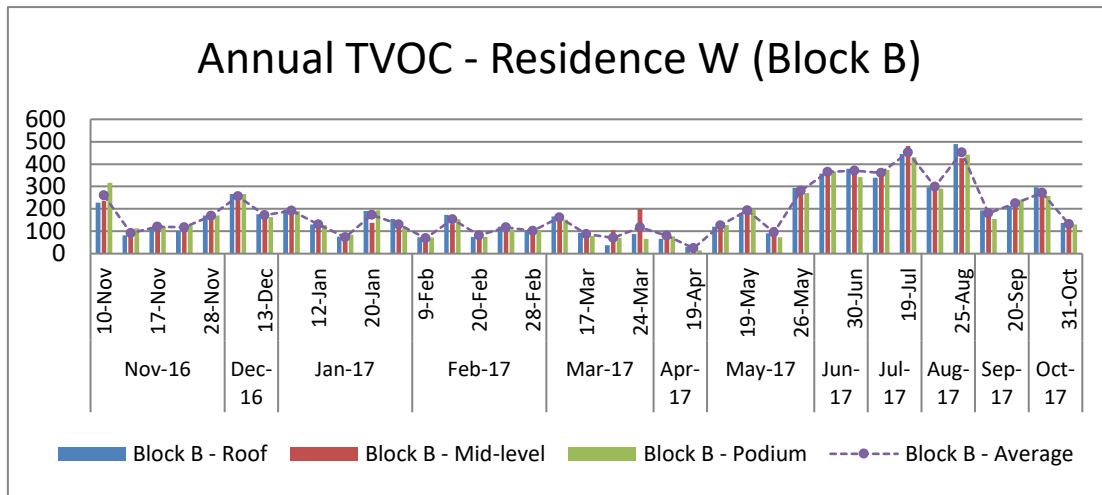
Figure 7c. Monthly levels of TVOC in Residence W (Block B)
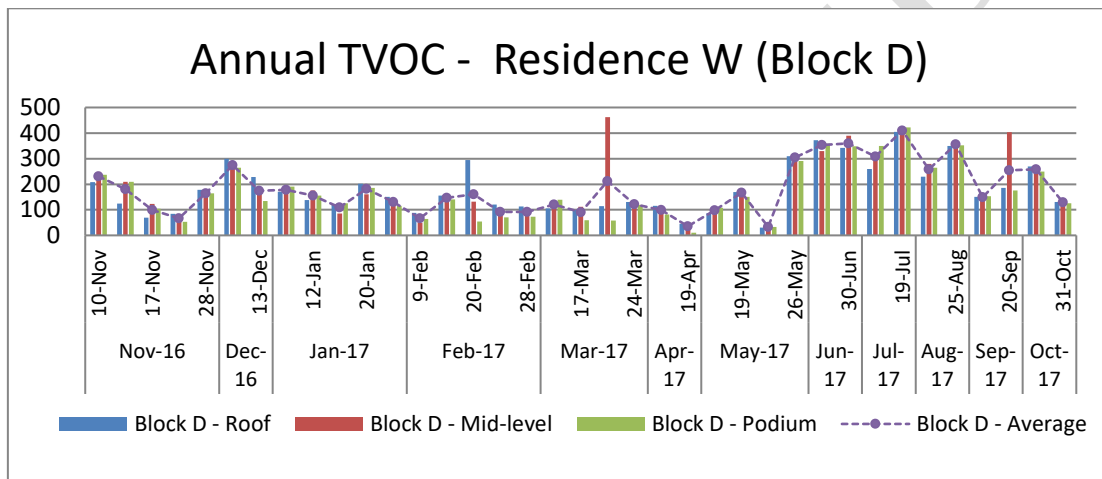
Figure 7d. Monthly levels of TVOC in Residence W (Block D)
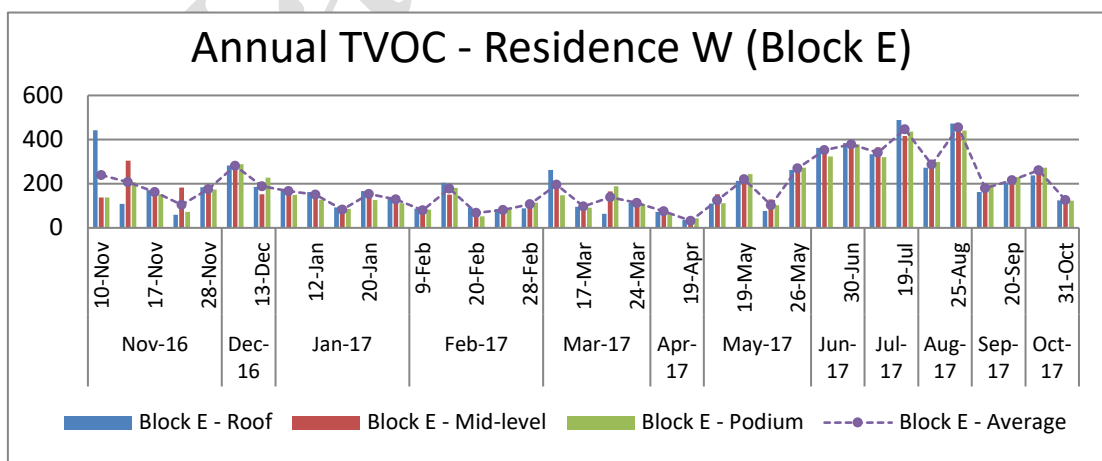
Figure 7e. Monthly levels of TVOC levels in Residence W (Block E)
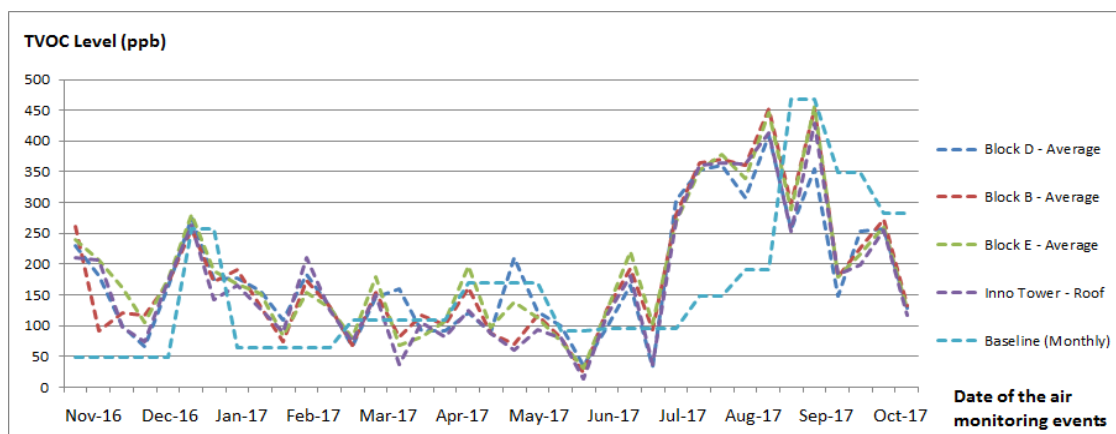
Figure 7f. Comparison of monthly average TVOC levels between baseline and operational air monitoring events

The baseline monitoring results revealed that the TVOC levels in Residence W ranged from 40 ppb to 485 ppb. TVOC concentration exceeding acute levels (i.e., > 435 ppb) were recorded in all monitoring locations during mid-summer. When compared with the Good Class IAQ level of TVOC (261 ppb), suggested by the IAQMG (2003), the limit in Block D was exceeded: four times on the roof, two times at the mid-level, and three times on the podium. The baseline monitoring results showed that the ambient TVOC levels within the district frequently exceeded 261 ppb. Figure 7f shows similar peaks and fluctuation patterns of TVOC levels in both baseline and operational (involving four buildings and ten sampling points) air monitoring events over the year.

It is worth noting that renovation activities were identified on the 8th, 10th, and 20th floors of Block E; 5th, 12th, 13th, and 14th floors of Block D; and 20th floor of Block B. High TVOC (> 435 ppb) values were recorded nearby these renovation points.

Therefore, it can be concluded that the construction/renovation activities in Residence W led to a substantial increase on the TVOC results of the field study.
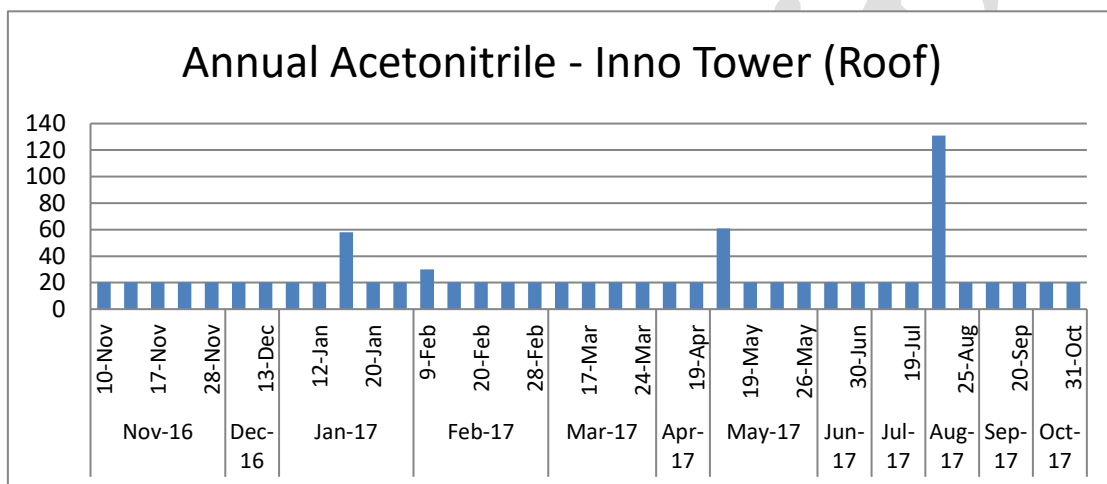
3.3 Acetonitrile

Fig. 8 presents the trend of acetonitrile levels measured in the baseline air monitoring (Fig. 8a), and the results of operational air monitoring for IT (Fig. 8b) and for Blocks B (Fig. 8c), D (Fig. 8d), and E (Fig. 8e) of Residence W. Fig. 8f combines the results obtained from both baseline and operational air monitoring. The field data revealed that acetonitrile levels were mostly within the limits with occasional peaks at different locations and different times irrespective of wind directions and laboratory activities in the ZS Building. Relatively high acetonitrile levels, higher than the chronic exposure level of 36 ppb, were observed at Residence W in crosswind, downwind, and upwind conditions. Therefore, no direct evidence was available to prove that the activities in the ZS Building contributed to the sporadic peaks recorded throughout the year. It is more likely that other nearby sources contributed to that.
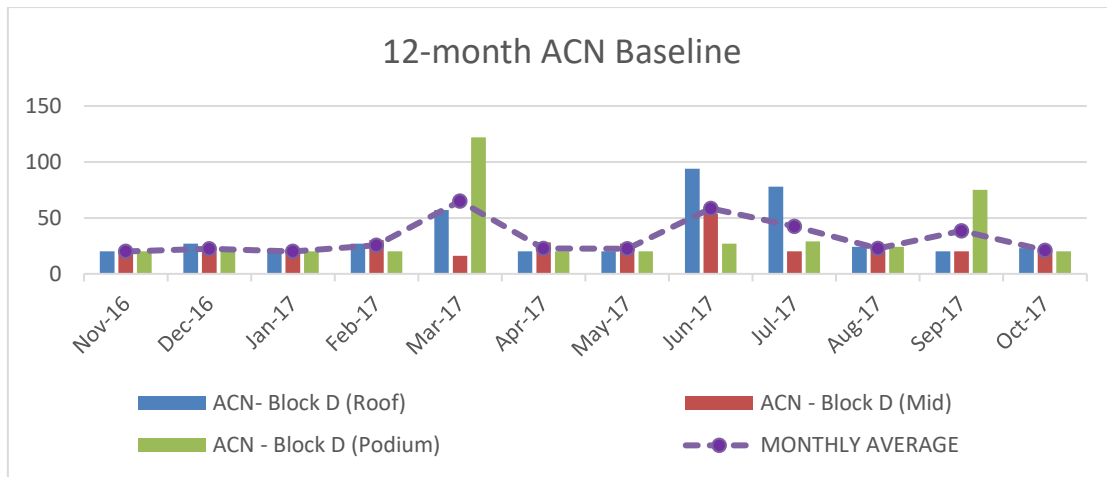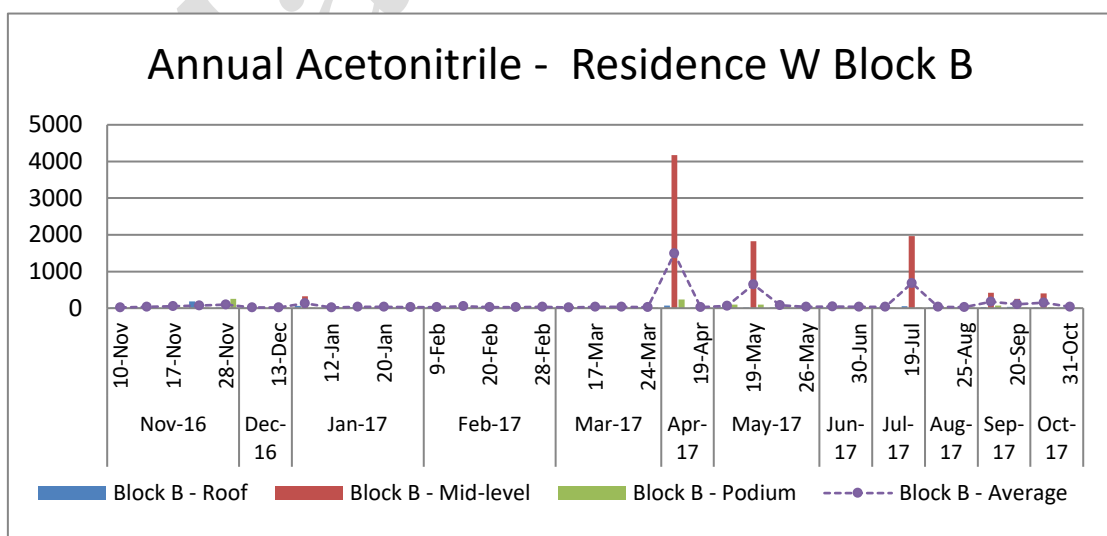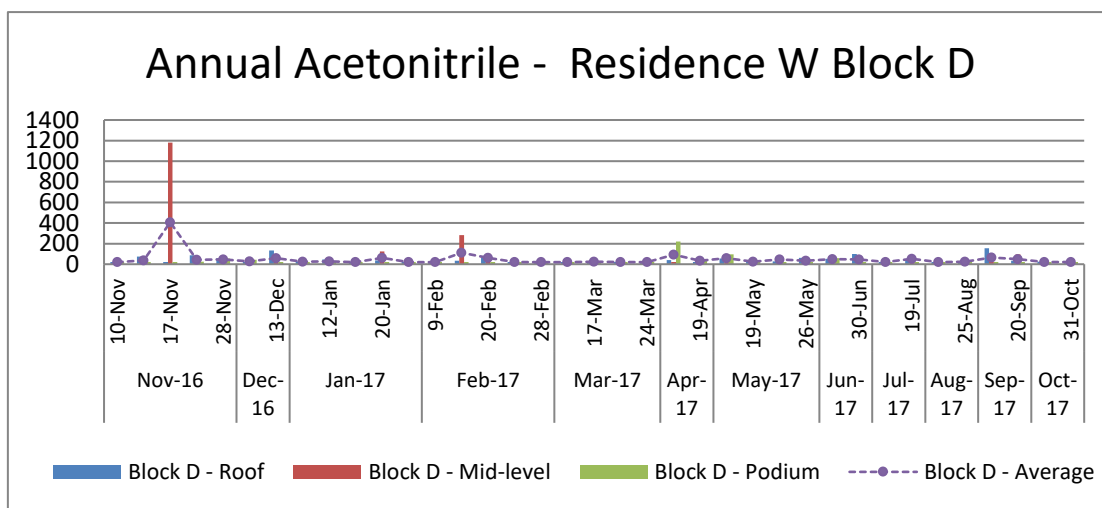
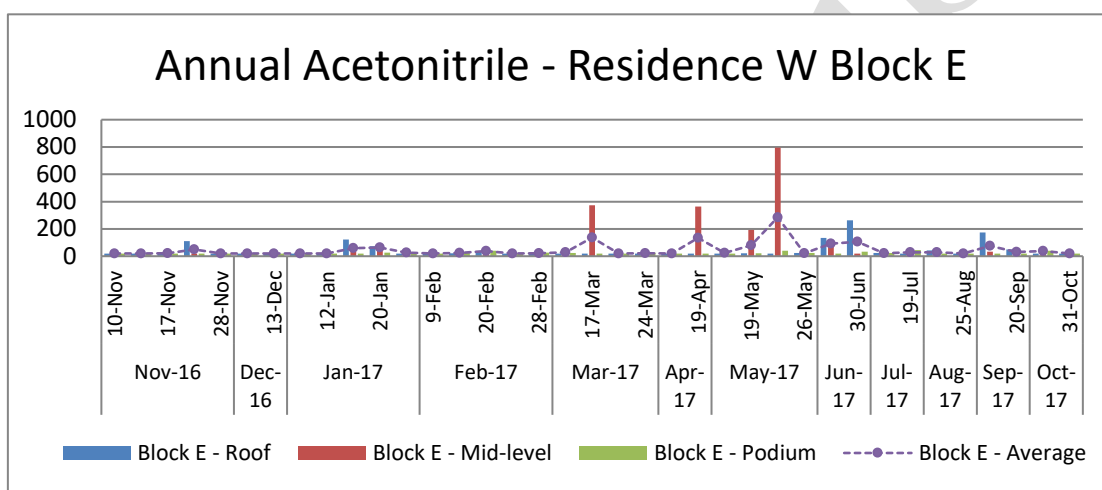*Figure 8a.   Twelve-month baseline acetonitrile (ACN) levels*

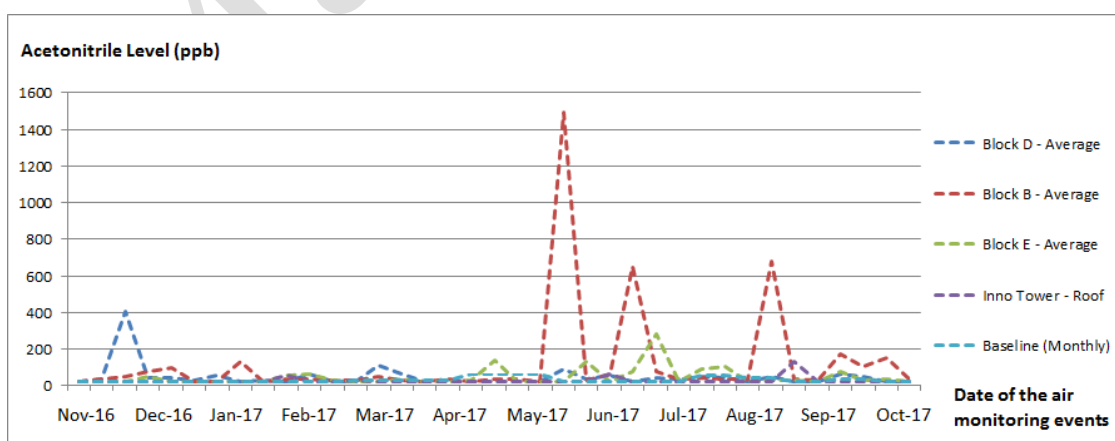*Figure 8b.   Monthly levels of acetonitrile in IT*

Figure 8c.   Monthly levels of acetonitrile in Residence W (Block B)

Figure 8d. *Monthly levels of acetonitrile in Residence W (Block D)*

Figure 8e. *Monthly levels of acetonitrile in Residence W (Block E)*

Figure 8f. *Comparison of monthly average acetonitrile levels between baseline and operational air monitoring events*

3.4   Trace Gas Study Results

To rule out the effect of environmental factors such as cigarette smoking, burning of materials, and renovation work nearby the air sampling stations, and to correctly identify the dilution effect within the urban setting for the gaseous emission from the stacks, a full-scale tracer gas study was conducted. The study identified the dilution factor of the environment and helped validate the simulation results produced by the CFD modelling.

The tracer gas study was performed when south eastern wind was dominant in the study area. The stack information and the measurement results are summarized in Tables 4 and 5, respectively.

Details of experimental setup	
Average Flue Gas Velocity (m/s)	2.7
Flue Gas Temperature (°C)	28.1*
SF_6 concentration inside stack (ppb)	2,823,000
Wind direction at source	Southeast (143°)
Wind-speed (m/s) at source	4
Ambient Temperature (°C)	28*
Tracer gas emission rate (g/s)	0.085

the average temperatures over the 30-minute tracer gas sampling

Table 4.   *Characteristics of the tracer gas emission*

Sampling Time	SF₆ Concentration (ppb)					
	Inside fume cupboard	In-stack (Source) C_e	Roof of ZS Building C	Block D (Podium) C	Block D (Mid) C	Block D (Roof) C
14:30 – 15:00	24,396,000	2,823,000	1 – 95 (15.8)	1 – 18 (4.3)	4 – 16 (10)	1 – 17 (4)
Dilution factors (D)			178,671	656,512	282,300	705,750

Note: Arithmetic means of 30-minute samplings, comprising six five-minute samplings, are given in brackets ( ).

Table 5.   Results of SF₆ monitoring (ppb) at various measurement locations

The emitted tracer gas was highly diluted by the environment before reaching the recipients in Residence W (Table 5). The dilution factors (D) ranged from 178,671 to 705,750. Despite the dilution, the concentration of the tracer gas at the mid-level was more than twice that on the podium and the roof of the building in Residence W. As mentioned, the sampling location for mid-level was on the leeward side of the building. The results demonstrate that the tracer gas was significantly diluted when it reached the roof and podium (windward sides) but somehow accumulated in the wake region of Residence W.

3.5 CFD Modelling Results

The RNG and RLZ *k*-ε turbulence models were used to generate simulation results for comparison with the tracer gas study results. Owing to the limitation of the tracer gas study set up in the residential buildings and the urban environment, only a few

experimental data could be used for the comparison. Table 6(a) and (b) summarize

the comparison amongst the data generated by the RNG k-ε model, the RLZ k-ε

model, and the tracer gas sampling.

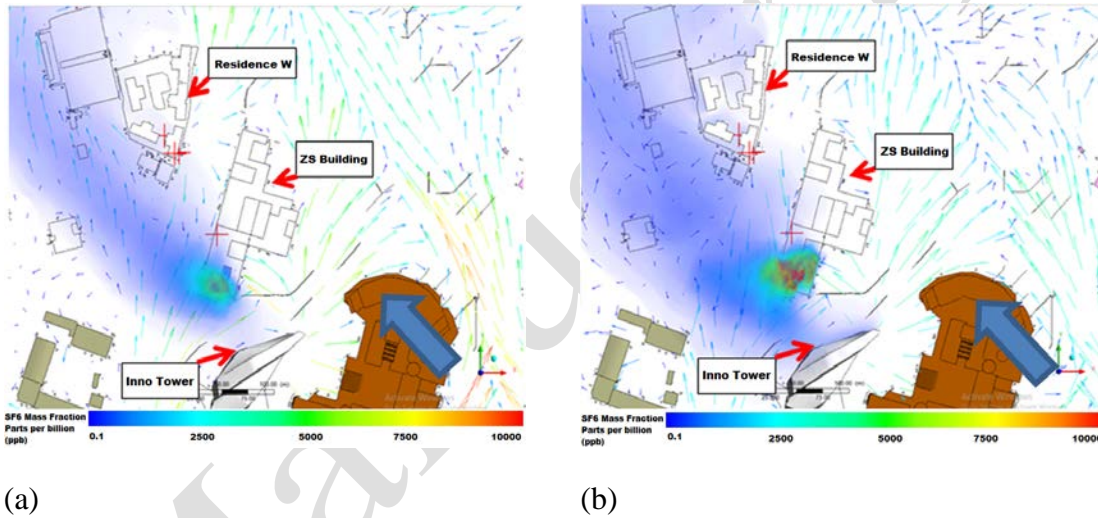| Location		Concentration of Tracer Gas (ppb)		Statistical Tests	
		Tracer Gas Sampling	RNG k-ε Data	MG	FAC2
Residence W	Block D (Roof)	4.00	2.66 (-33.5%)	1.50	0.67
	Block D (Pod.)	4.30	4.91 (+12.4%)	0.88	1.14
	Block D (Mid)	10.00	7.49 (-25.1%)	1.33	0.75
ZS Building	Roof	15.80	12.80 (-19.0%)	1.23	0.81

Notes: Acceptable ranges for MG and FAC2 are 0.7-1.3 and 0.5-2, respectively (Tewari et al., 2010)

Table 6(a).   Comparison between simulated results from RNG k-ε and tracer gas sampling results

Location		Concentration of Tracer Gas (ppb)		Statistical Tests	
		Tracer Gas Sampling	RLZ k-ε Data	MG	FAC2
Residence W	Block D (Roof)	4.00	5.86 (+46.5%)	0.68	1.47
	Block D (Pod.)	4.30	12.8 (+197.7%)	0.33	2.98
	Block D (Mid)	10.00	24.7 (+147%)	0.4	2.47
ZS Building	Roof	15.80	60.0 (+279.7%)	0.26	3.80

Notes: Acceptable ranges for MG and FAC2 are 0.7-1.3 and 0.5-2, respectively (Tewari et al., 2010)

Table 6(b).   Comparison between simulated results from RLZ k-ε and tracer gas sampling results

There were significant differences between the simulated data obtained by the RLZ k-ε model and the tracer gas sampling results (Table 6b). The MG for the RNG k-ε results ranged from 0.88 to 1.5 (acceptable range 0.7 – 1.3), which were better than the RLZ k-ε results of 0.26 – 0.68. The FAC2 for the RNG k-ε model ranged from 0.67 to 1.14, while the range for RLZ k-ε was between 1.47 and 3.8 (acceptable range: 0.5 – 2.0). The tracer gas concentration near the source (on the roof of the ZS Building) modeled by the RLZ k-ε was nearly 280% of the actual concentration. The results from the RLZ k-ε model statistically show a lesser agreement with the experimental results when compared to the RNG k-ε model. In general, the RLZ k-ε model overestimated the concentration of the tracer gas in all sampling locations, particularly at the building wake region and near the emission source. In contrast, the RNG k-ε model provides more accurate results with a narrower variation (-33.5% to 12.4%). The results from the RNG k-ε model agreed well with the tracer gas data for downstream (roof of the ZS Building) and windward side (Block D-Podium), but there was less agreement with the tracer gas concentration of the roof (MG: 1.5; FAC2: 0.67) and in the wake region (MG: 1.33; FAC2: 0.75) of Block D.

Fig. 9 illustrates the distribution and dispersion pattern of the tracer gas in the area of interest. Fig. 9a shows that the RLZ k-ε model produced a narrower lateral spread of tracer gas, while the RNG k-ε model in Fig. 9b demonstrates the

recirculation of tracer gas in the wake region and windward side of the ZS Building, and in the wake region of IT. The simulation by the RNG k-ε model shows that the concentration transport along the upwind direction by advection is dominant, and it is well represented by the concentration in the upwind region, which is between the ZS Building and IT (Fig. 9b). In this case, the air pollutants from the stack would be trapped and accumulate in the recirculation zone (enclosure of the buildings) in Residence W, and in the leeward of IT.

(a)   (b)

Notes: + denotes the locations of tracer gas sampling and ⬅ denotes the wind direction

***Figure 9.   Dispersion pattern of SF₆ simulated by (a) RLZ k-ε model and (b) RNG k-ε model***

Fig. 10 shows the ratio of mean concentration (C) and concentration of SF_6 at the emission source (C_0). A remarkable difference between the mean SF_6 concentration distribution of both RANS simulation approaches was observed. The RLZ k-ε model overestimates the tracer gas concentration on the windward wall (Fig. 10a) and the central enclosure (Fig. 10c) of Residence W, but it underestimates the concentration

distribution upstream, on the leeward wall of IT (Fig. 10b). In Fig. 10a, the concentration distribution on the windward wall of Residence W was considerably steady in the low- and mid-levels (from z = 30 to 50 m), and it gradually decreased to z = 50 m. Similarly, Fig. 10c shows that the concentration distribution within the central enclosure of Residence W was comparatively higher in the low- and mid-levels, and it weakened from z = 50 m upwards. However, Fig. 10b shows that concentration distributions gradually increased upward starting at z = 20 m on the leeward wall of IT, reaching a maximum at z = 70 m in RNG k-ε, and z = 50 m in RLZ k-ε. The gradual increasing concentration of tracer gas on the leeward wall of IT could be attributed to the weakening of effluent momentum of contaminants and flow velocities predicted by the models.
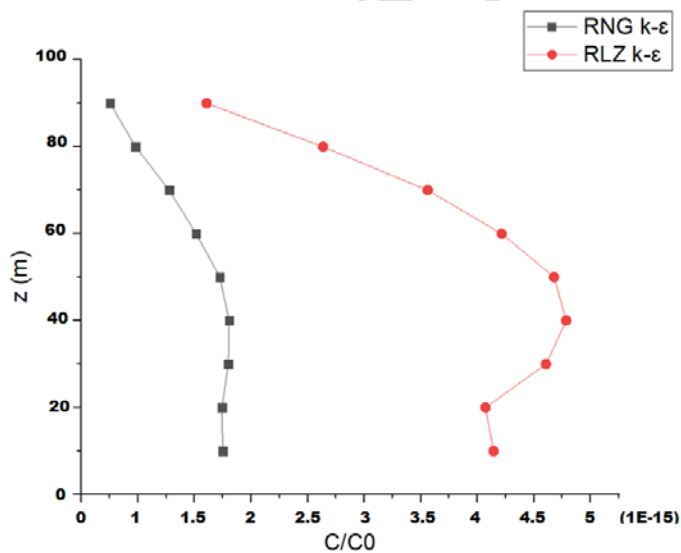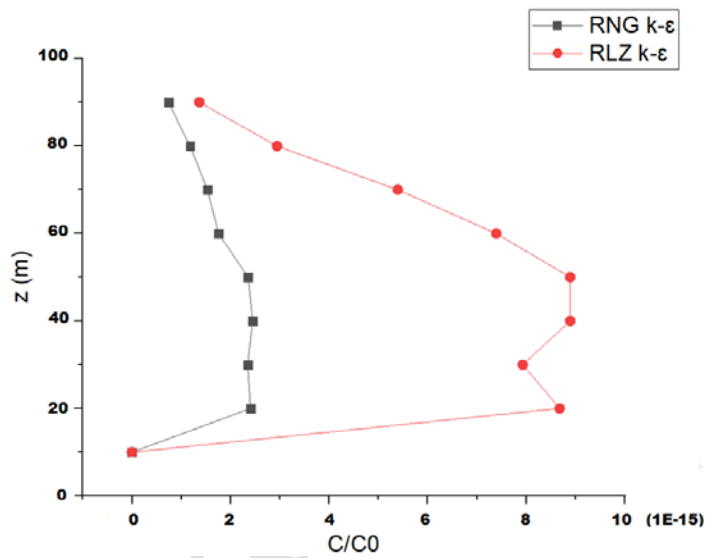

(a)
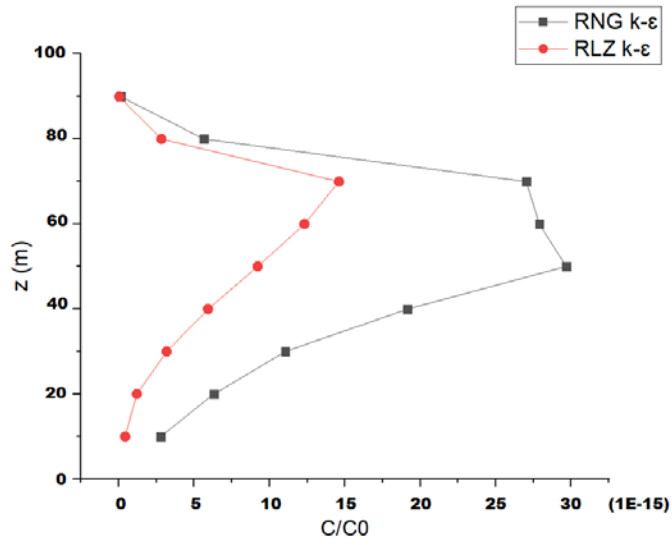
(b)

(c)

Figure 10. Mean concentration distribution of SF₆ at the: (a) windward wall of Block D in Residence W; (b) leeward of IT; (c) central enclosure of Residence W

As for the flow patterns, Fig. 11 illustrates the vertical flow patterns across the urban settings generated by the (a) RNG k-ε and (b) RLZ k-ε models. The recirculation flow predicted by the RNG k-ε model is stronger than the predicted by the RLZ k-ε. Fig. 11a also demonstrates that vortices were fully developed in the

wake regions of the IT, ZS Building, and Residence W. Fig. 11b shows that the turbulence vortex of the RLZ k-ε model at the wake region of IT was not well developed, and the reattachment length of turbulence was significantly longer. The lower wind-speeds in the recirculating enclosure could explain the SF_6 accumulation in these areas.

(a)
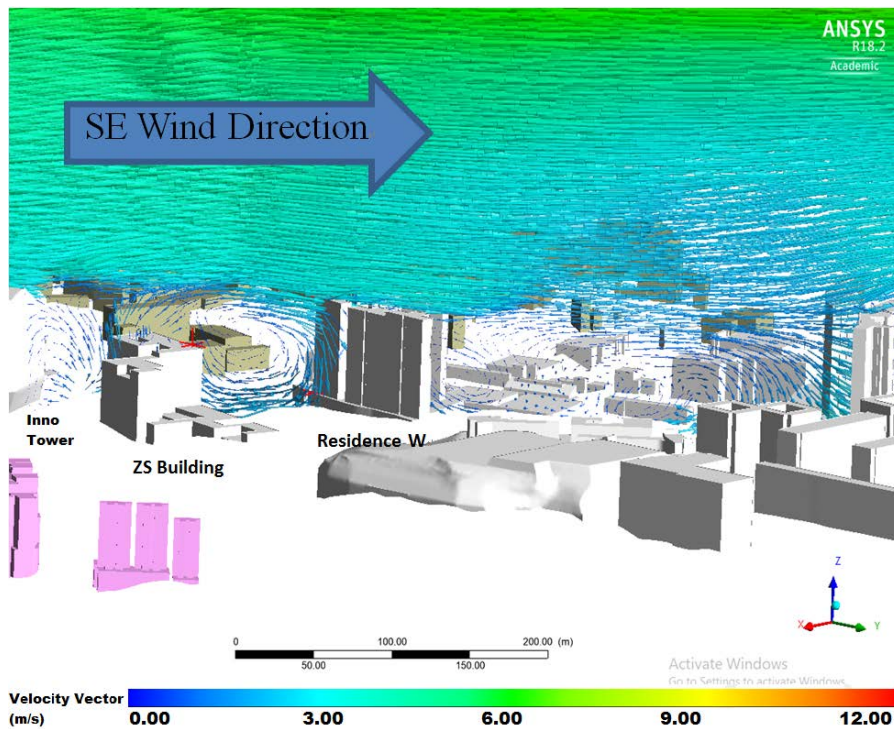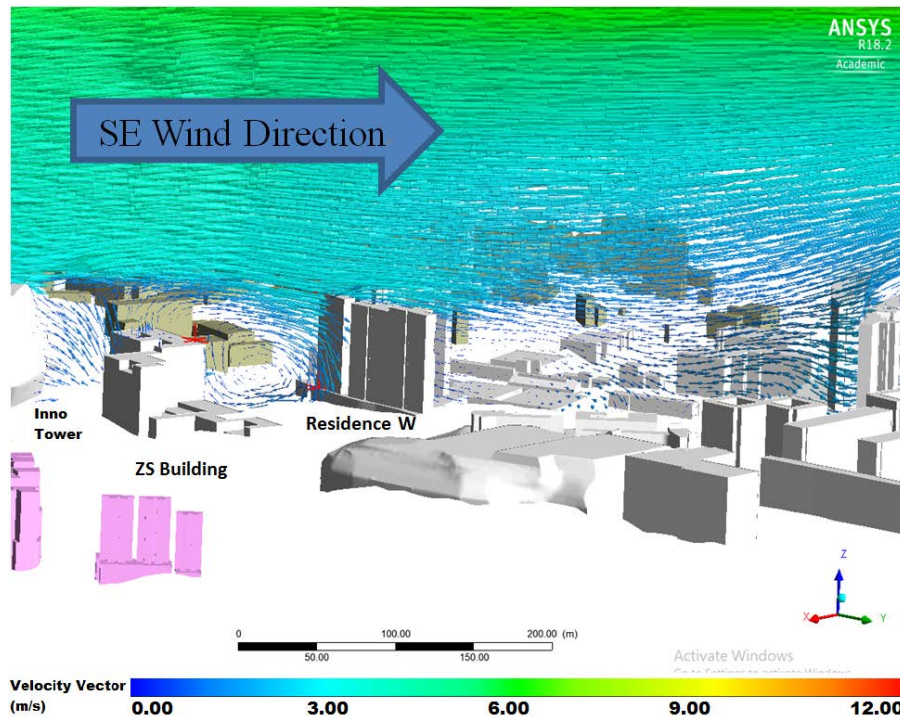
(b)

Figure 11.   Flow patterns within the building groups by (a) RNG k-ε and (b) RLZ k-ε models

Fig. 12 shows the horizontal planes and demonstrates that the air inside the central enclosure of the building group in Residence W is relatively stagnant. For most areas along the leeward wall facing the enclosure, airspeeds were approximately 0.5 m/s or lower. Fig. 12 also demonstrates that RNG has a wider horizontal range with higher wind speeds in the wake region of Residence W, which facilitated the clearance of air contaminants from this region. The velocity contours also show that the RNG k-ε model describes in greater detail the change in flow velocities in the central enclosure of Residence W and behind the buildings. The RLZ k-ε model shows a longer trail of low speeds and reattachment length behind the building.
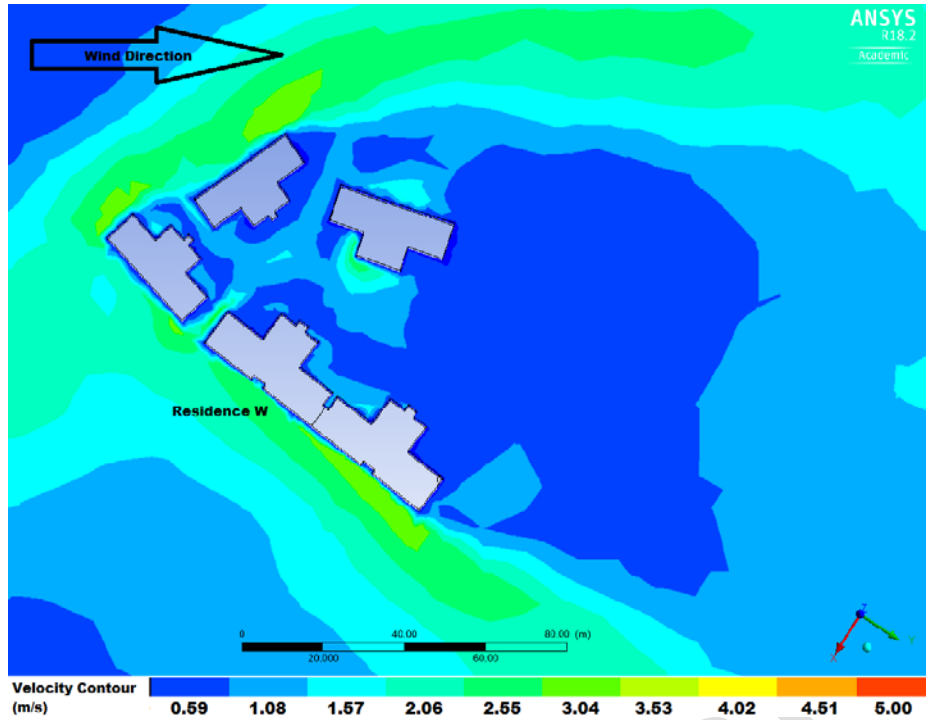
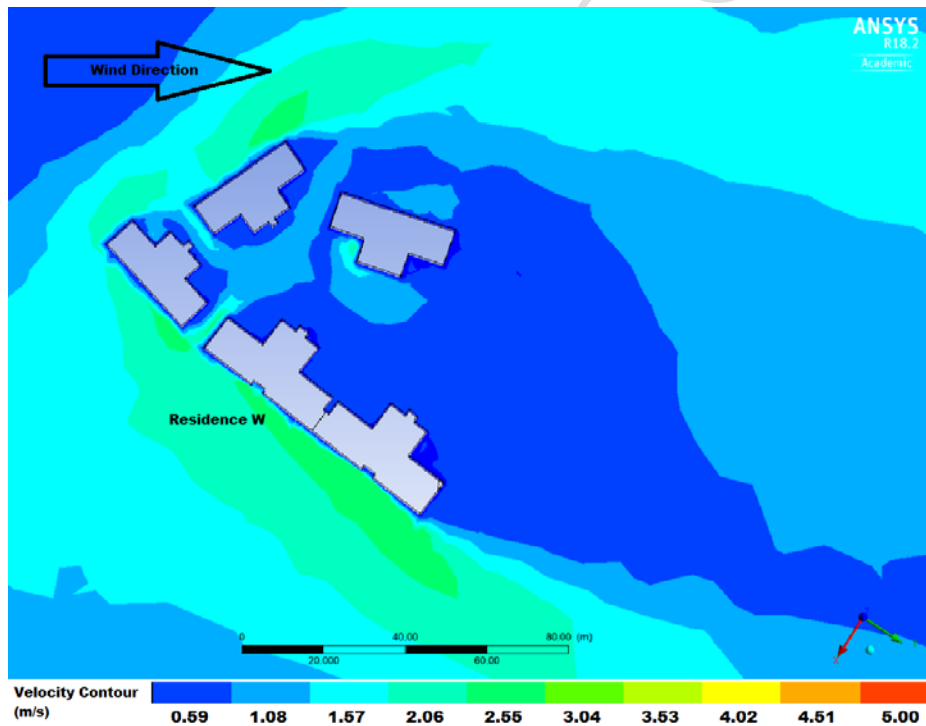*Figure 12a. Horizontal flow patterns and wind velocities at the mid-level of Residence W by the RNG-ε model*

*Figure 12b. Horizontal flow patterns and wind velocities at the mid-level of Residence W by the RLZ k-ε model*

In terms of the mean velocities (u/u_o), Fig. 13a shows that flow velocities on the

windward wall of Block D increased from the podium level up to z = 40 m. The RLZ

Page 44

k-ε model shows a negative value in the lower vertical level, indicating that a reverse flow was developed. The value gradually increases and peaks on the roof of the building. In contrast, the RNG *k*-ε model shows a slight decrease in velocity from z = 40 m to z = 70 m. The velocity increased at z = 80 m and reached its maximum on the roof of the building. The velocity ratio on roof of the building predicted by the RNG *k*-ε model is higher than that predicted by the RLZ *k*-ε. The velocity ratio obtained by RNG and RLZ *k*-ε models account for the difference between the two predicted tracer gas concentrations of both RANS simulation approaches.

The negative values in the mid- to upper-levels of IT (Fig. 13b) and the central enclosure of Residence W (Fig. 13c) indicate that there are reverse flows in the area and that turbulence accumulated. Both models display similar results along the leeward walls of IT. Either prevailing wind direction places IT upstream of the ZS Building, and the reverse flow indicates that IT could be affected by the emissions from the ZS Building regardless of the wind direction. In Fig. 13c, both models show similar reverse flow patterns in the central enclosure of Residence W, which favors the accumulation of air pollutants.
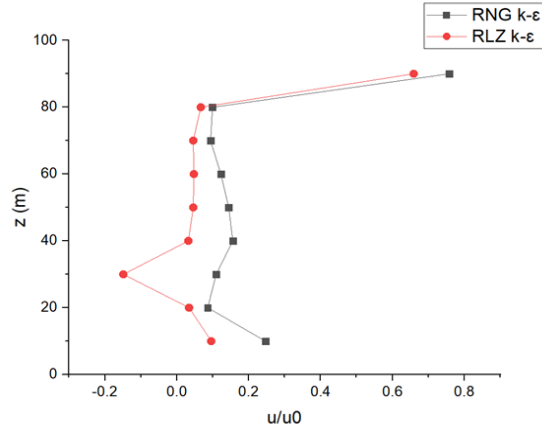
(a)
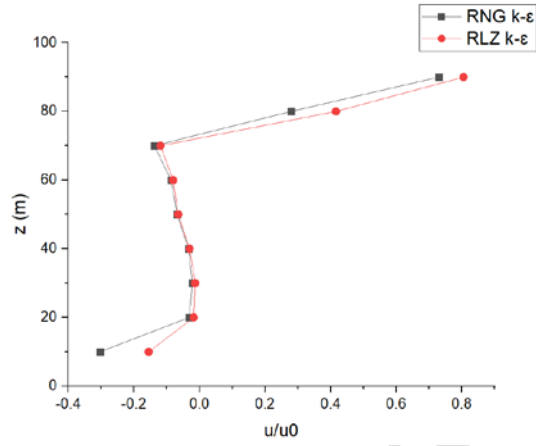
(b)
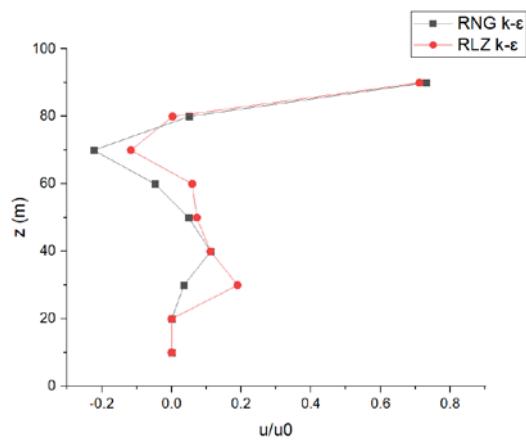
(c)

Figure 13. Mean wind-speed ratio on the (a) windward wall of Block D in Residence W; (b) leeward side of IT; (c) central enclosure of Residence W. Where u refers to the mean wind-speed at specific vertical locations, and u_0 refers to the inflow velocity at the boundary.

4. **Discussion**

Some chemical parameters, namely NO_2, TVOC, and acetonitrile, exceeded the predetermined exposure levels in both operational and baseline air monitoring. From the results of annual NO_2 levels in urban areas of Hong Kong, such as Central/Western and Eastern districts, Sham Shui Po, Kwai Chung, and Tsuen Wan, it was observed that NO_2 pollution was widely spread on the region, affecting the entire district throughout the year. Therefore, exceeding levels of NO_2 at Residence W and IT were possibly caused by the background contributions and not by the stacks on the roof of the ZS Building.

Levels of TVOC exceeding the acute concentration criterion were also recorded on the roof of Block E when the northeast wind was dominant. Therefore, it is suggested that these exceeding values were likely due to the upstream background rather than from emissions by the ZS Building. However, the exceeding levels recorded on the podium of Block B, and on the roof and podium of Block E under southeast winds were possibly due to the stack emission from ZS Building. According to a study performed in Korea, the concentration of VOCs near laboratory buildings can be significantly higher than the background concentrations outside non-laboratory buildings (Park et al., 2014). The obtained results could be attributed to the large amount of chemicals used during the normal operation of the laboratories and the absence of air-purification devices in the exhaust systems of these buildings.

There were only 7 (1.9%) high TVOC episodes (> 435 ppb) out of 370 monitoring events. These occurred in the mid-level of Block D; in the roof and mid-level of Block B; and in the roof, mid-level, and podium of Block E, when southeast wind was dominant. However, four out of these seven events occurred on the same day when the TVOC concentrations at IT were also high, despite IT being located in an upwind position. From the flow pattern simulated by the RNG k-ε model, recirculation and backflow took place at the wake regions of both IT and Residence W. That may have contributed to the elevated TVOC levels in the background of the whole district, and in the sampling locations of IT and building wakes in Residence W, irrespective of the wind direction.

As for acetonitrile, the baseline monitoring results revealed that the average hourly acetonitrile levels ranged from 20 ppb to 122 ppb for Residence W, and from 20 to 297 ppb for IT. A relatively high acetonitrile level, higher than the chronic exposure level of 36 ppb, at Residence W was observed under different wind directions. Amongst the 93 monitoring events with high acetonitrile levels, only 34 (36.6%) were recorded under downwind conditions (i.e., SE, SSE, and S), and of these, only four episodes involved the actual use of acetonitrile in the laboratories of the ZS Building, accounting for 4.3% of the occurrences of high acetonitrile levels. The highest acetonitrile level (4,170 ppb) was recorded in the mid-level of Block B

when northeast wind was dominant. Therefore, it is unlikely that this elevated

acetonitrile level derived from the gaseous emission by the ZS Building. In IT, the

exceedances occurred in the upwind and crosswind directions and had no apparent

association with the gaseous emission from the ZS Building, but the recirculation and

backflow, shown by the RNG k-ε model, may explain the elevated readings. However,

it was observed that cigarette smoke, particularly the smoke exhaled by smokers, may

also contribute to the increased atmospheric acetonitrile concentration. Typical

concentrations of acetonitrile in the breath range from 17 ppb to 126 ppb (Abbott,

Elder, Španěl, & Smith, 2003) and can reach up to 200 ppb (Jordan, Hansel,

Holzinger, & Lindinger, 1995). Hence, cigarette smoking nearby the sampling

location and equipment may have affected the overall sampling results.

The comparison between the results from the tracer gas study and the CFD

simulations showed that the RNG k-ε model is statistically better than the RLZ k-ε for

the prediction of tracer gas concentration, particularly for the sites near the source and

the windward side of the recipient building. This is consistent with the findings from

the previous studies, which established that the RNG k-ε model can accurately predict

the flow field in street canyon (Ai & Mak, 2017), whereas the RLZ k-ε model may

underestimate turbulent fluctuations around buildings and fails to fully represent the

unsteady vortex-shedding motion in the wake region (Tominaga & Stathopoulos,

2007). From the simulation by the RNG k-ε model (Fig. 9b), the concentration transport along the upwind direction by advection is dominant, and it is well represented by the concentration in the upwind region between the ZS Building and IT. In this case, the air pollutants from the stack would be trapped and accumulate in the recirculation zone (central enclosure of the buildings) of Residence W, and in the leeward of IT. This is also consistent with the findings from Lateb et al. (2013) and Tominaga and Stathopoulos (2013). The RNG k-ε model also elucidates the excursions of TVOC and acetonitrile in the air sampled from IT, even under the downwind situation (southeast wind), when IT was upwind of the stack emissions. In that case, the emissions may also have a potential impact on the overall IAQ in IT, since the fresh air intake of the MVAC system is located on the leeward wall of the building, facing the ZS Building.

From the simulation of tracer gas dispersions, it was found that the gradual increase of tracer gas concentration on the leeward wall of IT and Residence W could be attributed to the weakening of effluent momentum of contaminants and flow velocities. The wind-speeds in these regions were generally lower, and the flow recirculation was favorable for backflow and accumulation of air pollutants and it could explain the SF_6 accumulation in these areas. However, to ascertain the effect of flow turbulence on the distribution of air pollutants and tracer gas, scenarios with

different wind speed and incident angles should be modelled.

5. **Conclusions**

The gaseous emission from stacks connected to the fume cupboards of chemical laboratories may have detrimental health effects on the people working or living nearby. In a densely populated city such as Hong Kong, exposure to various air pollutants of anthropogenic sources is inevitable, difficult to identify, and contribute to the pollution load. This paper summarizes the results of an emission study in a comprehensive approach to identify the effects of gaseous emission from a laboratory building situated within a short distance from a residential building group in the Kowloon city, Hong Kong. Amongst the 15 selected chemicals, only NO_2, acetonitrile, and TVOC exceeded the predetermined exposure levels. Upon examination of the test results, wind directions, and the results of baseline monitoring activities, it was concluded that pre-existing environmental sources, such as renovation work in close proximity of air sampling locations may have contributed to the exceeding results of the air monitoring. However, the stack emissions from the ZS Building can also be assumed as accountable, particularly for the elevated results in IT and mid-level locations in Residence W. The tracer gas study results and CFD modelling indicate that the gaseous emissions were greatly diluted above the roof of the ZS Building.

The flow simulation by the RNG k-ε model demonstrated that the recirculation

vortices formed at the wake region or leeward side of the building further reduce the air-flow velocities. That subsequently enhanced the accumulation of pollutants, affecting the air quality in the urban area. Though IT is located upstream of the emission source, the simulated results from the RNG k-ε model also revealed that the concentration transport along the upwind direction by advection and recirculation flow would still affect IT. That could also explain the excursions of TVOC and acetonitrile in IT, irrespective of the wind direction. Therefore, the installation of fresh air intake on the leeward wall of IT should be avoided due to the potential for higher pollutant concentrations caused by the reverse flow in the building-wake region.

However, the validation process showed that RNG k-ε model could only achieve a relatively accurate prediction of pollutant dispersions in a real urban environment when compared with the RLZ k-ε model. Despite the RNG k-ε model yields statistically acceptable results with respect to all tracer gas sampling data according to the FAC2 (0.67-1.14), when it is challenged by the MG, it tends to over-estimate the pollutant concentrations on the rooftop (MG: 1.5) and leeward side of the recipient buildings (MG: 1.33).

Even though the RANS simulation approach is an economical choice in CFD simulations, the results from the present study show that it may not be sufficient to achieve statistically sound results with respect to the field measurement data collected in

a real urban environment. Careful interpretation of data generated by the RANS

approaches is hence needed, and it should be used and read in conjunction with the air

monitoring and tracer gas assessment data as a comprehensive approach when assessing

the impacts of stack emissions in the urban setting. In view of the insufficiency of

time-averaged simulation approaches like RANS used in the present study, other

transient models, such as Large Eddy Simulation (LES) and Detached Eddy Simulation

(DES), could be deployed to yield more accurate and realistic results. However, much

higher computational costs in terms of hardware and computing time would incur.

6.   **Acknowledgements**

7. **References**

Abbott, S. M., Elder, J. B., Španěl, P., & Smith, D. (2003). Quantification of

acetonitrile in exhaled breath and urinary headspace using selected ion flow

tube mass spectrometry. *International Journal of Mass Spectrometry, 228*(2),

655-665. doi:10.1016/S1387-3806(03)00212-4

Ai, Z. T., & Mak, C. M. (2013). CFD simulation of flow and dispersion around an

isolated building: Effect of inhomogeneous ABL and near-wall treatment.

Atmospheric Environment, 77, 568-578.

doi:https://doi.org/10.1016/j.atmosenv.2013.05.034

Ai, Z. T., & Mak, C. M. (2014). Modeling of coupled urban wind flow and indoor air

flow on a high-density near-wall mesh: Sensitivity analyses and case study for

single-sided ventilation. *Environmental Modelling and Software, 60*, 57-68.

doi:10.1016/j.envsoft.2014.06.010

Ai, Z. T., & Mak, C. M. (2016). Large eddy simulation of wind-induced interunit

dispersion around multistory buildings. *Indoor Air, 26*(2), 259-273.

doi:10.1111/ina.12200

Ai, Z. T., & Mak, C. M. (2017). CFD simulation of flow in a long street canyon under

a perpendicular wind direction: Evaluation of three computational settings.

Building and Environment, 114, 293-306.

doi:https://doi.org/10.1016/j.buildenv.2016.12.032

Ai, Z. T., Mak, C. M., & Lee, H. C. (2016). Roadside air quality and implications for

control measures: A case study of Hong Kong. *Atmospheric Environment, 137*,

6-16. doi:10.1016/j.atmosenv.2016.04.033

ANSYS FLUENT 14.5. (2012). Canonsburg, PA, USA: ANSYS, Inc.

ATSDR. (1994). Toxicological Profile for Acetone. Retrieved from

https://www.atsdr.cdc.gov/toxprofiles/TP.asp?id=5&tid=1

ATSDR. (1997). Toxicological Profile for Chloroform Retrieved from

https://www.atsdr.cdc.gov/toxprofiles/tp.asp?id=53&tid=16

ATSDR. (2006). *Toxicological Profile for 1,1,1-Trichloroethane*. Atlanta, GA.

ATSDR. (2017). Toxicological Profile for Toluene. Retrieved from

https://www.atsdr.cdc.gov/toxprofiles/tp.asp?id=161&tid=29

Ballinger, M. Y., & Larson, T. V. (2014). Source apportionment of stack emissions

from research and development facilities using positive matrix factorization.

Atmospheric Environment, 98, 59-65. doi:10.1016/j.atmosenv.2014.08.041

Blocken, B. (2015). Computational Fluid Dynamics for urban physics: Importance,

scales, possibilities, limitations and ten tips and tricks towards accurate and

reliable simulations. *Building and Environment, 91*, 219-245.

doi:https://doi.org/10.1016/j.buildenv.2015.02.015

Blocken, B., Janssen, W. D., & van Hooff, T. (2012). CFD simulation for pedestrian

wind comfort and wind safety in urban areas: General decision framework and

case study for the Eindhoven University campus. *Environmental Modelling &*

Software, 30, 15-34. doi:https://doi.org/10.1016/j.envsoft.2011.11.009

Blocken, B., Stathopoulos, T., & Carmeliet, J. (2007). CFD simulation of the

atmospheric boundary layer: wall function problems. *Atmospheric Environment,*

41(2), 238-252. doi:https://doi.org/10.1016/j.atmosenv.2006.08.019

Blocken, B., Stathopoulos, T., Saathoff, P., & Wang, X. (2008). Numerical evaluation

of pollutant dispersion in the built environment: Comparisons between models

and experiments. *Journal of Wind Engineering & Industrial Aerodynamics,*

96(10), 1817-1831. doi:10.1016/j.jweia.2008.02.049

Borrego, C., Martins, H., Tchepel, O., Salmim, L., Monteiro, A., & Miranda, A. I.

(2006). How urban structure can affect city sustainability from an air quality

perspective. *Environmental Modelling and Software, 21*(4), 461-467.

doi:10.1016/j.envsoft.2004.07.009

Bradshaw, P. (1969). The analogy between streamline curvature and buoyancy in

turbulent shear flow. *Journal of Fluid Mechanics, 36*(1), 177-191.

doi:10.1017/S0022112069001583

Burman, J., & Jonsson, L. (2015). Issues when linking computational fluid dynamics

for urban modeling to toxic load models: The need for further research.

Atmospheric Environment, 104, 112-124. doi:10.1016/j.atmosenv.2014.12.068

Canepa, E. (2004). An overview about the study of downwash effects on dispersion of

airborne pollutants. *Environmental Modelling and Software, 19*(12), 1077-1087.

doi:10.1016/j.envsoft.2003.11.011

Celik, I., Ghia, U., Roache, P., & Christopher. (2008). Procedure for estimation and

reporting of uncertainty due to discretization in CFD applications. *Journal of*

fluids {Engineering-Transactions} of the {ASME}, 130(7).

doi:citeulike-article-id:6537269

doi: 10.1115/1.2960953

Census and Statistics Department of Hong Kong. (2018). Hong Kong Statistics.

Population. Retrieved from

https://www.censtatd.gov.hk/hkstat/sub/sp150.jsp?tableID=001&ID=0&product

Type=8

Chan, T. L., Dong, G., Leung, C. W., Cheung, C. S., & Hung, W. T. (2002). Validation

of a two-dimensional pollutant dispersion model in an isolated street canyon.

Atmospheric Environment, 36(5), 861-872.

doi:https://doi.org/10.1016/S1352-2310(01)00490-3

Chang, J. C., & Hanna, S. R. (2004). Air quality model performance evaluation.

Meteorology and Atmospheric Physics, 87(1), 167-196.

doi:10.1007/s00703-003-0070-7

Cremades, L. (2000). Estimating the background air concentration excluding the

contribution of an individual source. *Environmental Modeling & Assessment,*

5(2), 119-124. doi:10.1023/A:1019057527154

Dadioti, R., & Rees, S. (2017). Performance of Detached Eddy Simulation applied to

analysis of a university campus wind environment. *Energy Procedia, 134*(C),

366-375. doi:10.1016/j.egypro.2017.09.551

Dai, Y., Mak, C. M., Ai, Z., & Hang, J. (2018). Evaluation of computational and

physical parameters influencing CFD simulations of pollutant dispersion in

building arrays. *Building and Environment, 137*, 90-107.

doi:10.1016/j.buildenv.2018.04.005

Dervos, C. T., & Vassiliou, P. (2000). Sulfur hexafluoride (SF6): global environmental

effects and toxic byproduct formation. *Journal of the Air & Waste Management*

Association, 50(1), 137.

Du, Y., & Mak, C. M. (2018). Improving pedestrian level low wind velocity

environment in high-density cities: A general framework and case study.

Sustainable Cities and Society, 42, 314-324.

doi:https://doi.org/10.1016/j.scs.2018.08.001

Du, Y., Mak, C. M., & Li, Y. (2019). A multi-stage optimization of pedestrian level

wind environment and thermal comfort with lift-up design in ideal urban

canyons. *Sustainable Cities and Society, 46*, 101424.

doi:https://doi.org/10.1016/j.scs.2019.101424

Fang, Z., Feng, X., Liu, J., Lin, Z., Mak, C. M., Niu, J., . . . Xu, X. (2019).

Investigation into the differences among several outdoor thermal comfort

indices against field survey in subtropics. *Sustainable Cities and Society, 44*,

676-690. doi:https://doi.org/10.1016/j.scs.2018.10.022

Franke, J., Hellsten, A., Schlünzen, H., & B. Carissimo. (2007). *Cost Action 732: Best*

Practice Guideline for the CFD Simulation of Flow in the Urban Environment,

in: Quality Assurance and Impovement of Microscale Meteorological Models, .

Gao, N. P., Niu, J. L., Perino, M., & Heiselberg, P. (2008). The airborne transmission

of infection between flats in high-rise residential buildings: Tracer gas

simulation. *Building and Environment, 43*(11), 1805-1817.

doi:https://doi.org/10.1016/j.buildenv.2007.10.023

Garbrecht, O. (2017). *Large Eddy Simulation of Three-dimensional Mixed Convection*

on a Vertical Plate. (Doctor of Engineering approved dissertation), RWTH

Aachen University,

Gousseau, P., Blocken, B., Stathopoulos, T., & van Heijst, G. J. F. (2011). CFD

simulation of near-field pollutant dispersion on a high-resolution grid: A case

study by LES and RANS for a building group in downtown Montreal.

Atmospheric Environment, 45(2), 428-438.

doi:10.1016/j.atmosenv.2010.09.065

HKEPD. (2015). Air Quality Objectives. Retrieved from

http://www.epd.gov.hk/epd/english/environmentinhk/air/air_quality_objectives/

air_quality_objectives.html

HKEPD. (n.d.). Annual AQI Trend. Retrieved from

http://www.aqhi.gov.hk/en/annual-aqi/annual-aqi-trendfb71.html?stationid=74

Hong Kong Observatory. (2017). *Summary of Meteorological and Tidal Observations*

in Hong Kong 2016. Retrieved from

https://www.hko.gov.hk/publica/pubsmo.htm

Ignatius, M., Wong, N. H., & Jusuf, S. K. (2015). Urban microclimate analysis with

consideration of local ambient temperature, external heat gain, urban

ventilation, and outdoor thermal comfort in the tropics. *Sustainable Cities and*

Society, 19, 121-135. doi:https://doi.org/10.1016/j.scs.2015.07.016

Indoor Air Quality Management Group. (2003). *A Guide on Indoor Air Quality*

Certification Scheme for Offices and Public Places. Hong Kong: The

Government of Hong Kong Special Administrative Region.

Jordan, A., Hansel, A., Holzinger, R., & Lindinger, W. (1995). Acetonitrile and benzene

in the breath of smokers and non-smokers investigated by proton transfer

reaction mass spectrometry (PTR-MS). *International Journal of Mass*

Spectrometry and Ion Processes, 148(1), L1-L3.

doi:10.1016/0168-1176(95)04236-E

Koutsourakis, N., Bartzis, J. G., & Markatos, N. C. (2012). Evaluation of Reynolds

stress, k-ε and RNG k-ε turbulence models in street canyon flows using various

experimental datasets. *Environmental Fluid Mechanics, 12*(4), 379-403.

doi:10.1007/s10652-012-9240-9

Lübcke, H., Schmidt, S., Rung, T., & Thiele, F. (2001). Comparison of LES and RANS

in bluff-body flows. *Journal of Wind Engineering & Industrial Aerodynamics,*

89(14), 1471-1485. doi:10.1016/S0167-6105(01)00134-9

Lateb, M., Masson, C., Stathopoulos, T., & Bédard, C. (2011). Effect of stack height

and exhaust velocity on pollutant dispersion in the wake of a building.

Atmospheric Environment, 45(29). doi:10.1016/j.atmosenv.2011.06.040

Lateb, M., Masson, C., Stathopoulos, T., & Bedard, C. (2013). Comparison of various

types of k- epsilon models for pollutant emissions around a two-building

configuration. *Journal of Wind Engineering and Industrial Aerodynamics,*

115(C), 9-21. doi:10.1016/j.jweia.2013.01.001

Li, X.-X., Liu, C.-H., Leung, D. Y. C., & Lam, K. M. (2006). Recent progress in CFD

modelling of wind field and pollutant transport in street canyons. *Atmospheric*

Environment, 40(29), 5640-5658.

doi:https://doi.org/10.1016/j.atmosenv.2006.04.055

Li, Y., & Stathopoulos, T. (1997). Numerical evaluation of wind-induced dispersion of

pollutants around a building. *Journal of Wind Engineering and Industrial*

Aerodynamics, 67-68, 757-766.

doi:https://doi.org/10.1016/S0167-6105(97)00116-5

Liu, J., & Niu, J. (2016). CFD simulation of the wind environment around an isolated

high-rise building: An evaluation of SRANS, LES and DES models. *Building*

and Environment, 96(C), 91-106. doi:10.1016/j.buildenv.2015.11.007

Mirzaei, P. A., & Rad, M. (2013). Toward design and fabrication of wind-driven

vehicles: Procedure to optimize the threshold of driving forces. *Applied*

Mathematical Modelling, 37(1), 50-61.

doi:https://doi.org/10.1016/j.apm.2011.11.037

Mochida, A., & Lun, I. Y. F. (2008). Prediction of wind environment and thermal

comfort at pedestrian level in urban area. *Journal of Wind Engineering &*

Industrial Aerodynamics, 96(10), 1498-1527. doi:10.1016/j.jweia.2008.02.033

Mu, D., Gao, N., & Zhu, T. (2016). Wind tunnel tests of inter-flat pollutant

transmission characteristics in a rectangular multi-storey residential building,

part A: Effect of wind direction. *Building and Environment, 108*, 159-170.

doi:https://doi.org/10.1016/j.buildenv.2016.08.032

Nathanson, T. (1995). *Indoor Air Quality in Office Buildings: A Technical Guide*.

    Canada: Health Canada, Minister of Supply and Services.

Niu, J., & Tung, T. C. W. (2008). On-site quantification of re-entry ratio of ventilation

    exhausts in multi-family residential buildings and implications. *Indoor Air,*

    18(1), 12-26. doi:10.1111/j.1600-0668.2007.00500.x

OEHHA. (2016). OEHHA Acute, 8-hour and Chronic Reference Exposure Level (REL)

    Summary. Retrieved from

    https://oehha.ca.gov/air/general-info/oehha-acute-8-hour-and-chronic-reference

    -exposure-level-rel-summary

Park, J., Lee, L., Byun, H., Ham, S., Lee, I., Park, J., . . . Yoon, C. (2014). A study of

    the volatile organic compound emissions at the stacks of laboratory fume hoods

    in a university campus. *Journal of Cleaner Production, 66*(C), 10-18.

    doi:10.1016/j.jclepro.2013.11.024

Shirzadi, M., Naghashzadegan, M., & A. Mirzaei, P. (2018). Improving the CFD

    modelling of cross-ventilation in highly-packed urban areas. *Sustainable Cities*

    and Society, 37, 451-465. doi:https://doi.org/10.1016/j.scs.2017.11.020

Tewari, M., Kusaka, H., Chen, F., Coirier, W. J., Kim, S., Wyszogrodzki, A. A., &

    Warner, T. T. (2010). Impact of coupling a microscale computational fluid

    dynamics model with a mesoscale model on urban scale contaminant transport

and dispersion. *Atmospheric Research, 96*(4), 656-664.

doi:https://doi.org/10.1016/j.atmosres.2010.01.006

Tominaga, Y., & Stathopoulos, T. (2007). Turbulent Schmidt numbers for CFD analysis

with various types of flowfield. *Atmospheric Environment, 41*(37), 8091-8099.

doi:https://doi.org/10.1016/j.atmosenv.2007.06.054

Tominaga, Y., & Stathopoulos, T. (2009). Numerical simulation of dispersion around

an isolated cubic building: Comparison of various types of k–ε models.

Atmospheric Environment, 43(20), 3200-3210.

doi:https://doi.org/10.1016/j.atmosenv.2009.03.038

Tominaga, Y., & Stathopoulos, T. (2013). CFD simulation of near-field pollutant

dispersion in the urban environment: A review of current modeling techniques.

Atmospheric Environment, 79(C), 716-730.

doi:10.1016/j.atmosenv.2013.07.028

USEPA- Integrated Risk Information System (IRIS). (2013). Chemical Assessment

Summary. Methanol; CASRN 67-56-1. Retrieved from

https://cfpub.epa.gov/ncea/iris2/chemicalLanding.cfm?substance_nmbr=305

USEPA-Integrated Risk Information System (IRIS). (1995). Chemical Assessment

Summary. Hydrogen chloride; CASRN 7647-01-0. Retrieved from

https://cfpub.epa.gov/ncea/iris2/chemicalLanding.cfm?substance_nmbr=396

USEPA-Integrated Risk Information System (IRIS). (2005). Chemical Assessment

Summary. n-Hexane; CASRN 110-54-3. Retrieved from

https://cfpub.epa.gov/ncea/iris2/chemicalLanding.cfm?substance_nmbr=486

USEPA-Integrated Risk Information System (IRIS). (2012). Chemical Assessment

Summary. Tetrahydrofuran; CASRN 109-99-9. Retrieved from

https://cfpub.epa.gov/ncea/iris2/chemicalLanding.cfm?substance_nmbr=1023

USEPA - Integrated Risk Information System (IRIS). (1999). Chemical Assessment

Summary. Acetonitrile. CASRN 75-05-8. Retrieved from

https://cfpub.epa.gov/ncea/iris2/chemicalLanding.cfm?substance_nmbr=205

USEPA - Integrated Risk Information System (IRIS). (2005). Chemical Assessment

Summary. Toluene; CASRN 108-88-3. Retrieved from

https://cfpub.epa.gov/ncea/iris2/chemicalLanding.cfm?substance_nmbr=118

USEPA - Integrated Risk Information System (IRIS). (2011). Chemical Assessment

Summary. Dichloromethane. CASRN 75-09-2. Retrieved from

https://cfpub.epa.gov/ncea/iris2/chemicalLanding.cfm?substance_nmbr=70

USEPA. (2014). Acute Exposure Guideline Levels (AGEL) for Selected Airborne

Chemicals Vol.16. Retrieved from

https://www.epa.gov/aegl/acetonitrile-results-aegl-program

Wieringa, J. (1992). Updating the Davenport roughness classification. *Journal of Wind*

Engineering and Industrial Aerodynamics, 41(1), 357-368.

doi:https://doi.org/10.1016/0167-6105(92)90434-C

World Health Organisation. (2000). *Air Quality Guidelines for Europe* (2 ed.).

Copenhagen: World Health Organization Regional Office for Europe.

Xia, Q., Niu, J., & Liu, X. (2014). Dispersion of air pollutants around buildings: A

review of past studies and their methodologies. In (Vol. 23, pp. 201-224).

London, England.

Yassin, M. F. (2013). A wind tunnel study on the effect of thermal stability on flow and

dispersion of rooftop stack emissions in the near wake of a building.

Atmospheric Environment, 65, 89-100.

doi:https://doi.org/10.1016/j.atmosenv.2012.10.013

Yuan, C., Ng, E., & Norford, L. K. (2014). Improving air quality in high-density cities

by understanding the relationship between air pollutant dispersion and urban

morphologies. *Building and Environment, 71*(C), 245-258.

doi:10.1016/j.buildenv.2013.10.008